ESD-TR-87-051

Annual Report

# Electrooptical Devices

30 September 1984

**Lincoln Laboratory**

MASSACHUSETTS INSTITUTE OF TECHNOLOGY

*LEXINGTON, MASSACHUSETTS*

**Prepared for the Department of the Air Force**
**under Electronic Systems Division Contract F19628-85-C-0002.**

The work reported in this document was performed at Lincoln Laboratory, a center for research operated by Massachusetts Institute of Technology, with the support of the Rome Air Development Center under Air Force Contract F19628-85-C-0002.



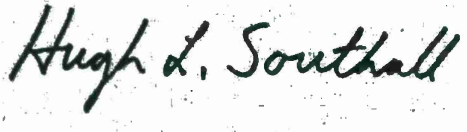

Hugh L. Southall, Lt. Col., USAF
Chief, ESD Lincoln Laboratory Project Office

MASSACHUSETTS INSTITUTE OF TECHNOLOGY
LINCOLN LABORATORY

# ELECTROOPTICAL DEVICES

ANNUAL REPORT
TO THE
ROME AIR DEVELOPMENT CENTER

1 OCTOBER 1983 — 30 SEPTEMBER 1984

ISSUED 23 FEBRUARY 1988



LEXINGTON MASSACHUSETTS

# ABSTRACT

This report covers work carried out with support of the Rome Air Development Center during the period 1 October 1983 through 30 September 1984.

GaInAsP/InP buried-heterostructure lasers formed by thermally transported InP have resulted in low threshold, high efficiency, and high device yield. Zinc diffusion has been utilized to improve the light-current linearity and reduce the threshold temperature dependence.

A technique has been developed to calculate the voltage and current distributions in the mass-transported GaInAsP/InP buried-heterostructure lasers. It is valuable for designing lasers for operation without current leakage through the InP pn homojunctions formed in the transported regions.

Mass-transported GaInAsP/InP buried-heterostructure lasers with low threshold currents and a linear light output to greater than 13 mW per facet have been obtained. This is achieved by using sufficient p-doping in the cap layer of the starting double-heterostructure wafer.

Buried-heterostructure, actively Q-switched diode lasers have been made with threshold currents as low as 14 mA. The lasers operate continuously at room temperature. Full on/off modulation has been observed at measurement-limited rates of about 12.6 GHz, while modulation has been seen at rates of 13.5 GHz.

The InP mass-transport technique has been used to improve chemically etched mirrors for GaInAsP/InP buried-heterostructure lasers. Devices with one such mirror and a second cleaved mirror show high device yield, threshold currents as low as 5 mA, and differential quantum efficiency as high as 33 percent.

# TABLE OF CONTENTS

# LIST OF ILLUSTRATIONS

## LIST OF TABLES

# ELECTROOPTICAL DEVICES

## I. NEW DEVELOPMENTS IN MASS-TRANSPORTED GaInAsP/InP BURIED-HETEROSTRUCTURE LASERS

As a potentially very important class of sources in fiber optical communication and integrated optics, GaInAsP/InP buried-heterostructure (BH) lasers have received much attention in recent years. By using liquid-phase epitaxial (LPE) regrowth techniques[1,2] or LPE growth on grooved substrates,[3-6] many groups of researchers have obtained BH lasers with excellent characteristics, such as low-threshold, high efficiency, high power operation, and high device yield. In a recent publication,[7] we reported promising preliminary results of a new BH laser in which thermally transported InP was used to form the burying sidewalls. This technique is simpler than the previously used techniques; it opens up new possibilities for integrated optoelectronic devices. In this section we report further development of the technique which has resulted in thresholds as low as 5.5 mA and device yields as high as 80 percent. In addition, Zn diffusion has been performed after the transport of InP and has resulted in improved linearity of the light-current characteristics and a $T_0$ of 81 K.

The fabrication procedure illustrated in Figure I-1 is essentially the same as described earlier;[7] only the new developments will be detailed in this report. Lasers parallel to either (011) or (011) planes have been fabricated. Except for Wafer 513, lasers reported here are parallel to (011) planes. To form the structure shown in Figure I-1(a), two narrow stripes were etched to form a mesa for the laser with large unetched supporting mesas (not shown in Figure I-1) on each side. The supporting mesas served to mechanically protect the laser mesas. Improved dimensional control of the quaternary active region width has been achieved with yet another kind of mesa which was 1.5 $\mu$m narrower than, but otherwise identical to, the laser mesas. The quaternary etching was terminated when these mesas were completely etched through. By using this technique, GaInAsP active regions 0.5 to 2.5 $\mu$m in width were routinely obtained. The transport of InP was carried out at temperatures between 600° and 670°C, depending on the desired amount of transport. The wafer was then loaded into an ampoule along with some zinc-phosphide powder. Two different modes of Zn diffusion have been used in different experiments. In the first mode, a Zn-skin diffusion was used to reduce contact resistance. The wafer was coated with phosphosilicate glass (PSG), photolithographically processed to form stripe openings on the mesa tops, and diffused at 600°C for 2.5 min. to form heavily doped regions in the stripe openings. In the second mode, a deep Zn diffusion was used to modify the cap doping profile as illustrated in Figure I-1(c). The wafer was uncoated and was diffused first at 450°C for 160 to 196 min., and then at 600°C for 2.5 min. Figure I-2 shows an SEM photograph of a stained cross section of a sample thus diffused. Except for the two most recent wafers (584 and 586), all other wafers reported here were only skin-diffused.

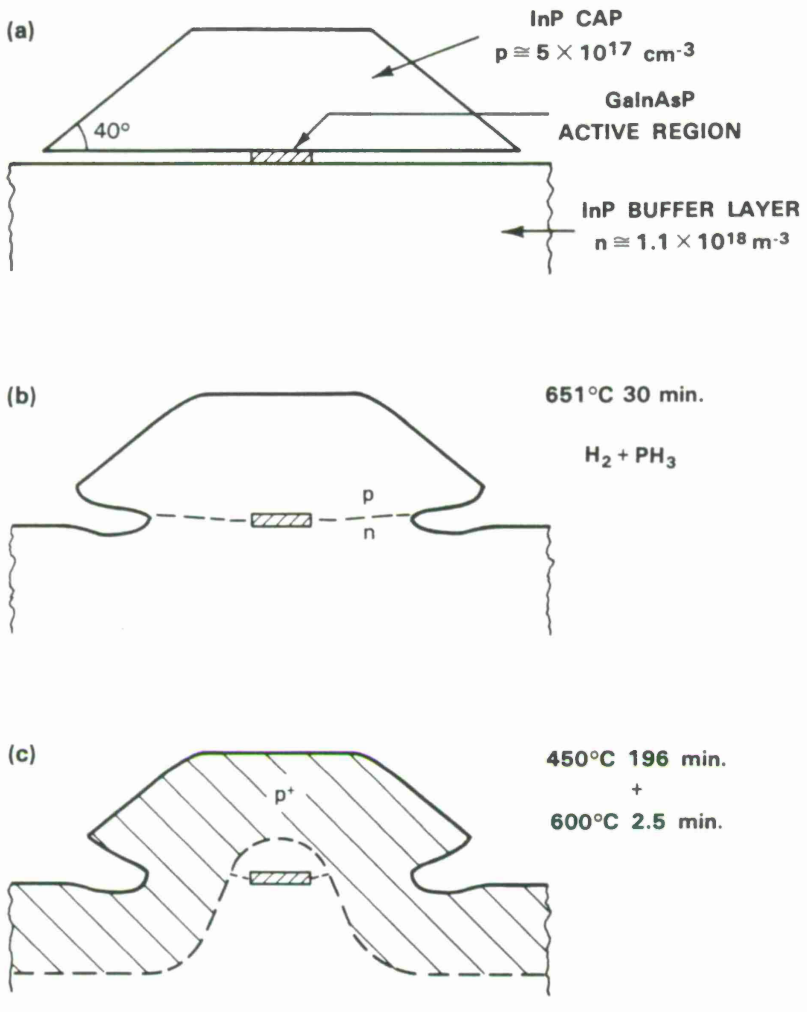


85890-1

*Figure I-1. Fabrication procedure of GaInAsP/InP BH laser with deep Zn-diffusion. The figure shows wafer after (a) selective chemical etching, (b) transport of InP, and (c) Zn diffusion.*

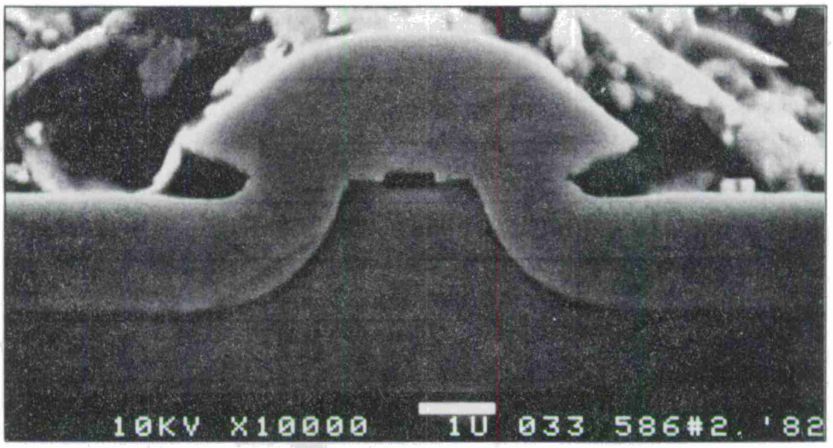


85890-2

*Figure I-2. SEM photograph of a stained cross section of BH after deep Zn-diffusion. In this sample, active region is 0.7 μm wide.*

Since the supporting mesas were first implemented, high device yield has been routinely obtained. For example, 80 percent of the 130 devices tested for Wafer 551 showed threshold currents between 10 and 30 mA. The lowest threshold was 5.5 mA, obtained for Wafer 514. The highest differential quantum efficiency was 27 percent per facet, obtained on a device of Wafer 513 with active regions of 3.0- to 3.6-$\mu$m width and a threshold current of 17 mA. The light-current (L-I) characteristics, however, typically exhibited deviations from linearity slightly above threshold, as shown in Figure I-3(a).

This deviation from linearity is presumably due to current leakage across the pn homojunctions, whose locations, based on SEM observations of stained cross sections, are shown in Figure I-1(b). The current leakage can be prevented either by increasing the conductivity of the p-type InP cap or by locating the pn homojunctions in low-voltage regions. In this work, both of the above-mentioned solutions were achieved by the deep Zn diffusion as illustrated in Figure I-1(c). Since high Zn-concentration in or near the active region has been known to greatly increase the laser threshold,[8,9] the deep Zn diffusion in this work is designed so that a lightly doped core region is retained for laser action.

Two wafers with deep Zn diffusion have been fabricated. Typical threshold currents were in the range of 12 to 30 mA. These devices showed significantly improved L-I linearity [Figure I-3(b)]. Improved temperature dependence of threshold current, $T_o$ = 81 K, was also obtained as compared with $T_o$ = 46 to 67 K without deep Zn diffusion. The differential quantum efficiencies were typically 17 percent per facet, which is lower than the best obtained on devices without the deep diffusion and may be due to the stripe unevenness observed on these two wafers. Deep Zn diffusion is a simple and effective method to improve the L-I linearity and $T_o$ in the mass-transported BH lasers without the use of reverse-biased junctions.

Z.L. Liau
J.N. Walpole
D.Z. Tsang

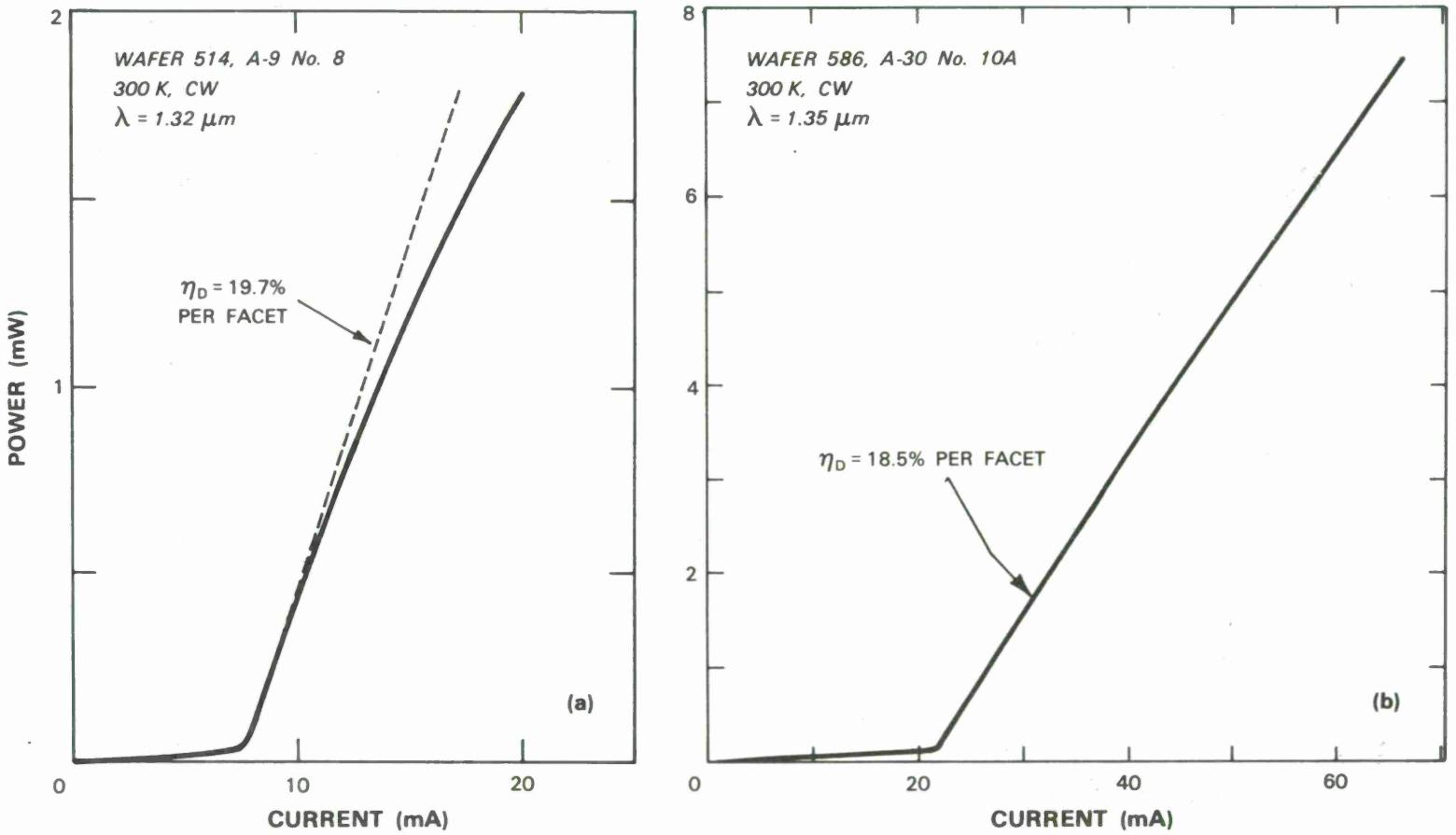


*Figure I-3. L-I characteristics of BH lasers (a) without and (b) with deep Zn-diffusion.*

85890-3

# II. THEORY OF VOLTAGE AND CURRENT DISTRIBUTIONS IN MASS-TRANSPORTED GaInAsP/InP BURIED-HETEROSTRUCTURE LASERS

A technique has been developed to calculate the voltage and current distributions in the mass-transported GaInAsP/InP buried-heterostructure laser. Consider the current flowing from the ohmic contact on top of a laser mesa such as that shown in Figure II-1. When the current is relatively low, it flows predominantly through the active region with only a negligibly small portion flowing through the InP pn homojunctions, because the quaternary has an energy gap smaller than that of InP. This current-flow pattern and the corresponding voltage distribution in the laser mesa has been analyzed by using a conformal mapping technique, the Schwarz-Christoffel transformation, to be described in this section. The forward-bias voltages along the InP pn homojunctions are obtained from this analysis and can be used to check if the homojunction current indeed remains negligibly small. Thus, the present calculation scheme is valuable in predicting the current limit within which the laser can be operated without leakage through the homojunctions.

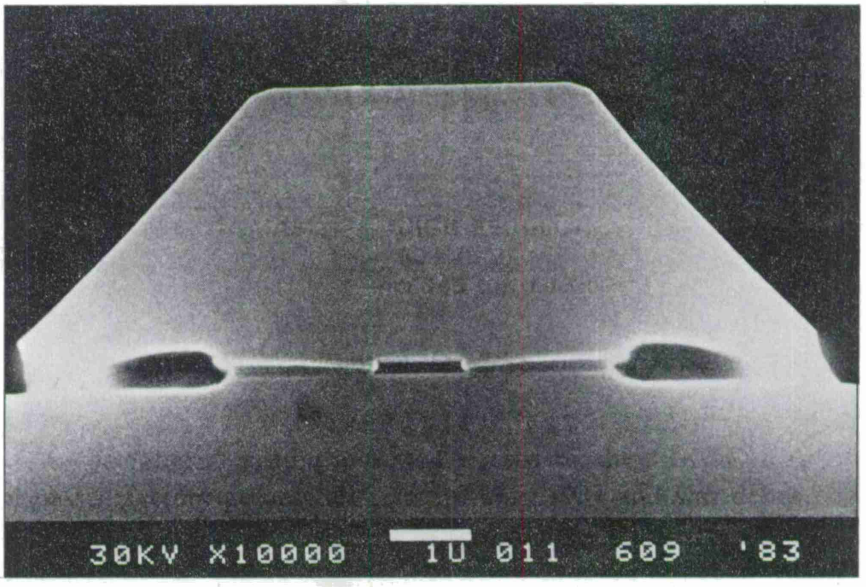


85890-4

*Figure II-1. SEM cross-sectional view of a laser mesa showing the formation of InP pn homojunctions in the transported regions. Steps seen in the transported regions are due to the staining procedure which preferentially eroded n-InP, as confirmed by rotating the sample during the SEM examination.*

As illustrated in Figures II-2 and II-3, the cross section of the laser mesa is approximated as a trapezoidal region with base angles of $\alpha = 0.927$ rad (=53°) in the upper complex w-plane ($w = u + iv$). The active region is approximated as an equipotential line segment (from $w = -W$ to $w = W$). Another equipotential is near the ohmic contact on the mesa top. In addition, no current is allowed to flow across the mesa sidewalls and the InP pn homojunctions. These boundary conditions are to be satisfied by the potential $\Phi(u,v)$. The latter is obtained by transforming a known potential $\Phi(x,y)$ from the upper complex z-plane ($z = x + iy$).

The potential $\Phi(x,y)$ in Figure II-2(b) is that of a two-dimensional current flow from infinity into a slit opening[10,11] which has a width from $z = -1$ to $z = 1$ and is maintained at a constant potential of $\Phi = 0$. The equipotentials are confocal ellipses, with foci at $z = -1$ and $z = 1$, and are given by

$$\frac{x^2}{\cosh^2 \Phi} + \frac{y^2}{\sinh^2 \Phi} = 1 \tag{1}$$

The upper complex z-plane is transformed into the triangular region in the upper complex w-plane in Figure II-2(a) by[10,11]

$$w = K \int_0^z (z' + a')^{(\alpha/\pi)-1} (z' - a')^{(\alpha/\pi)-1} \, dz' \tag{2}$$

where K and a′ are constants and are determined by requiring the mapping of $z = 1$ and a′ to $w = W$ and a, respectively.

By evaluating Equations (1) and (2) numerically, $\Phi(u,v)$ is obtained. Some examples are shown in Figures II-2(a) and II-3. [The equipotentials in Figure II-3 are labeled in V which is related to $\Phi$ by Equation (3) to be discussed below.] Note the equipotentials near the mesa tops are curved, and one of them will approximately coincide with the front of the Zn skin-diffused $p^+$ region.

The potential $\Phi(u,v)$ is then converted into the voltage distribution V(u,v) by using

$$V(u,v) = \frac{\rho \, I_Q}{\pi L} \, \Phi(u,v) + V_Q \tag{3}$$

where $\rho$ and L are the resistivity and device length, respectively, and $I_Q$ and $V_Q$ are the current flowing through and the junction voltage at the quaternary region, respectively. Equation (3) is obtained by letting $V(u,v) = \text{constant} \times \Phi(u,v) + V_Q$ and by requiring $L/\rho \int_{-W}^{W} (\partial V/\partial v]_{v=0} \, du = I_Q$. The junction voltage $V_Q$ is computed to be 0.98 V, by using published values of the band-structure parameters and threshold carrier density.[12,13]

Figure II-3 shows examples of calculated V(u,v). In these calculations and others to follow, $L = 300$ $\mu$m and $\rho = (pq \, \mu_p)^{-1}$ with $\mu_p = 70$ cm$^2$/(V - s) were used. The voltage distribution may now be used to estimate the current $I_H$ due to the forward-biased InP homojunctions. The homojunctions are approximated as ideal diodes, and $I_H$ is assumed to be dominated by the electron

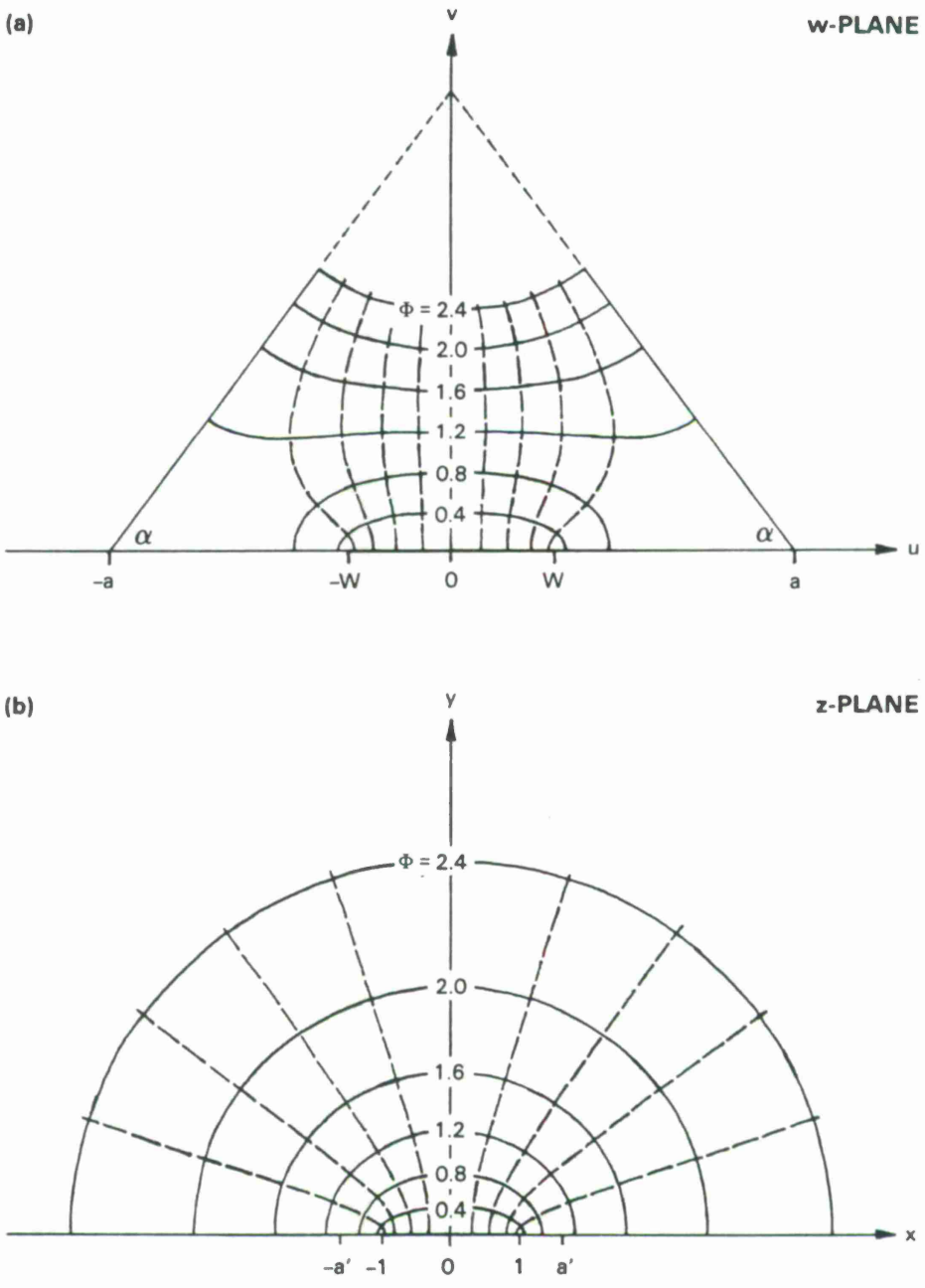


85890-5

*Figure II-2. The Schwarz-Christoffel transformation used to obtain the potential $\Phi(u,v)$ in the laser mesa. Dashed curves are the streamlines.*

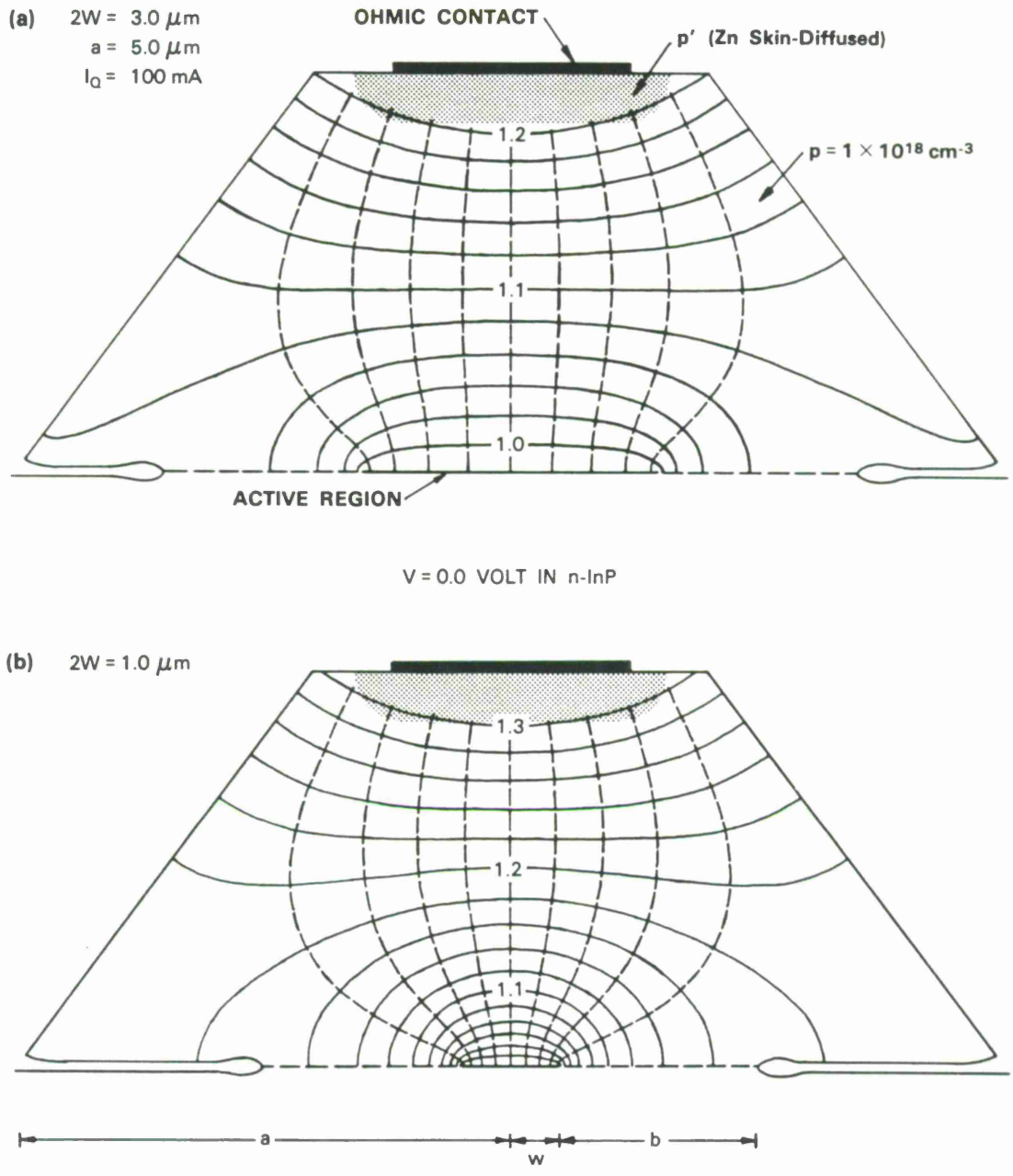


*Figure II-3. Calculated voltage distribution for two laser mesas with different active region widths. Equipotentials are separated by equal voltage increments; numbers are in volts. Dashed curves are the streamlines.*

injection into the p-InP cap region, since the n-InP buffer layer is generally more heavily doped and electrons have considerably higher diffusivity than holes. Therefore,

$$I_H = q \frac{A_H D_n}{L_n} \frac{n_i^2}{P} \exp[qV_H/kT] \quad (4)$$

where $A_H$ is the effective homojunction area, $D_n$ and $L_n$ are electron diffusivity and effective diffusion length, respectively, $n_i$ is the intrinsic carrier concentration, k is the Boltzmann constant, and $V_H = V(W + b,o)$ with b being the transported region width. The effective homojunction area is defined as $A_H = 2L\Delta b$, with the effective width $\Delta b = \int_W^{W+b} \exp [qV(u,o)/kT] du/\exp [qV_H/kT]$, which can be estimated to be approximately the distance in which V(u,o) reduces by kT/q or (as done here) evaluated precisely by numerical integration. In the following calculations $D_n = 78$ cm$^2$/s and $n_i^2 = 1.6 \times 10^{14}$ cm$^{-6}$ were used, as computed from published carrier-transport and band-structure parameters,[13] and a constant $L_n = 7$ $\mu$m was assumed.

Table II-1 shows calculated $I_H$ and related physical parameters as a function of $I_Q$ on a given device. Note that $I_H$ is initially very small but increases exponentially. When $I_H \simeq I_Q$, voltage along the InP homojunctions calculated for $I_Q$ alone may remain a fair approximation, because the additional electric field for the hole-drift-current component of $I_H$ is small up to approximately one electron-diffusion length away from the homojunctions and is therefore not expected to significantly affect the homojunction voltage. The effect of the calculated homojunction current on an otherwise linear L-I characteristic is demonstrated in Figure II-4, which was

**TABLE II-1**

**Calculated $I_H$ and Related Parameters as a Function of $I_Q$ for $p = 4 \times 10^{17}$ cm$^{-3}$, $a = 5.0$ $\mu$m, $W = 1.5$ $\mu$m, and $b = 2.0$ $\mu$m**

| $I_Q$ (mA) | $V_H$ (V) | $\Delta b$ ($\mu$m) | $n_p(0)^*$ (cm$^{-3}$) | $I_H$ (mA) | $I_1$ (mA) | $I_2$ (mA) |
|---|---|---|---|---|---|---|
| 20 | 1.03 | 1.37 | $7.15 \times 10^{13}$ | 0.0732 | 53.9 | 12.9 |
| 40 | 1.08 | 1.08 | $4.56 \times 10^{14}$ | 0.368 | 52.3 | 12.2 |
| 60 | 1.13 | 0.87 | $3.03 \times 10^{15}$ | 1.96 | 52.0 | 11.9 |
| 80 | 1.17 | 0.75 | $1.93 \times 10^{16}$ | 10.9 | 52.3 | 11.6 |
| 100 | 1.22 | 0.65 | $1.28 \times 10^{17}$ | 62.0 | 52.7 | 11.5 |

* $n_p(0) \times \frac{n_i^2}{p} \exp [qV_H/kT]$

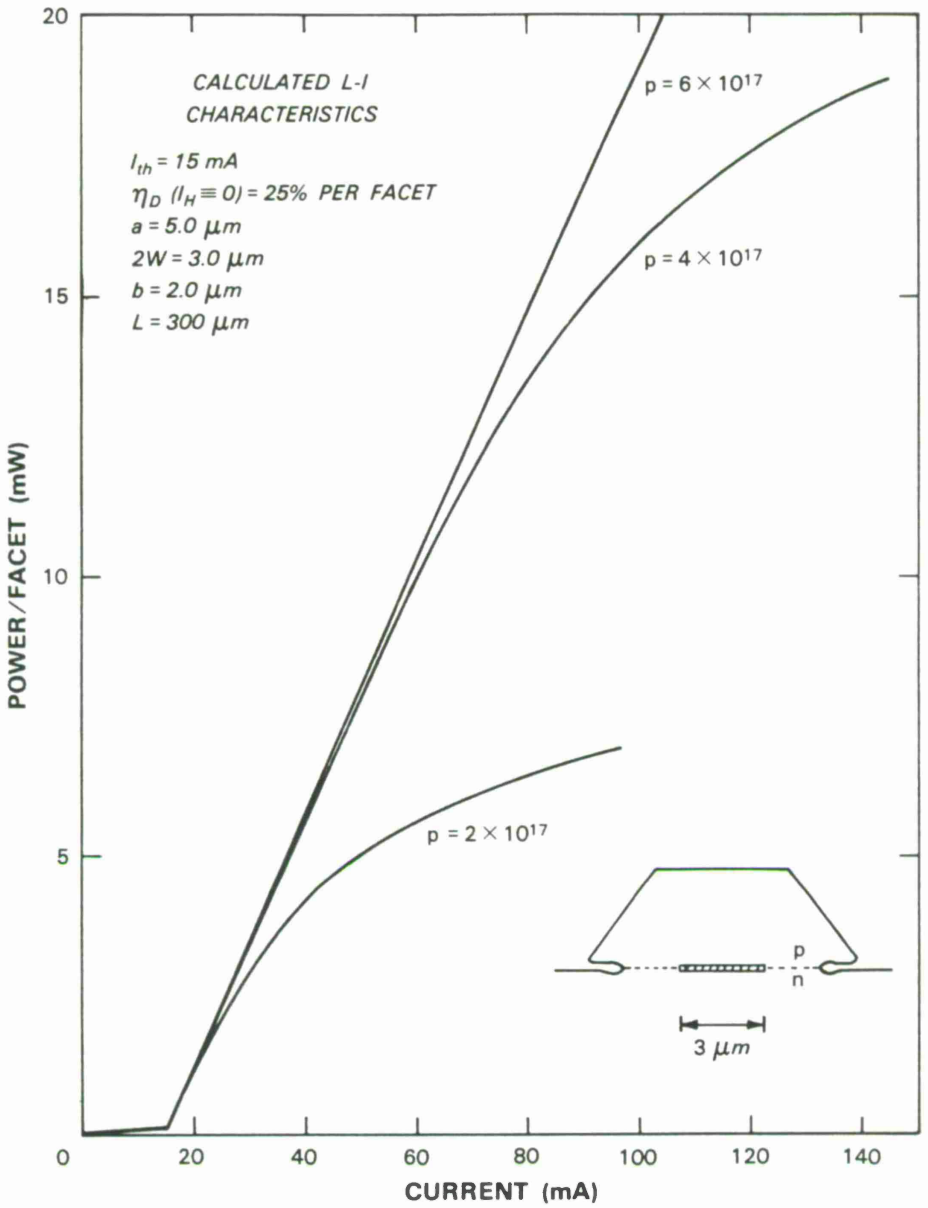


85890-7

*Figure II-4. Sublinear L-I characteristics resulting from adding the homojunction current to a linear one. Calculation of the homojunction current was carried out for the device geometry shown in the insert and for three different p-doping concentrations. Note that the numerical values of the curve of $p = 4 \times 10^{17}$ $cm^{-3}$ are listed in Table II-1.*

obtained by adding $I_H$ to $I_Q$ for each power output. To facilitate comparison with experiment, Equations (3) and (4) can be combined and rearranged into

$$I_H = 1 \text{ mA} \cdot \exp [(I_Q - I_1)/I_2] \quad (5)$$

where $I_1$ and $I_2$ are parameters characteristic of the device and are nearly independent of $I_Q$ (cf. Table II-1). Note that $I_1$ is essentially the value of $I_Q$ at which $I_H$ becomes significant ($I_H$ = 1 mA). The functional form of Equation (5) is in good agreement with experiment.

Figure II-5 shows calculated $I_1$ as a function of p for a = 5.0 $\mu$m, b = 2.0 $\mu$m and three values of W. The experimental values of $I_1$ for $p \leqslant 3 \times 10^{17}$ cm$^{-3}$ were 15 to 26 mA, in general agreement with Figure II-5. A more accurate comparison, however, is not available at present because of the uncertainties in both theory and experiment.

In conclusion, the conformal mapping technique allows for rather accurate calculation of the voltage distribution in the laser mesa. The present theory is valuable for designing lasers for operation without current leakage through the forward-biased homojunctions.

Z.L. Liau
J.N. Walpole
D.Z. Tsang

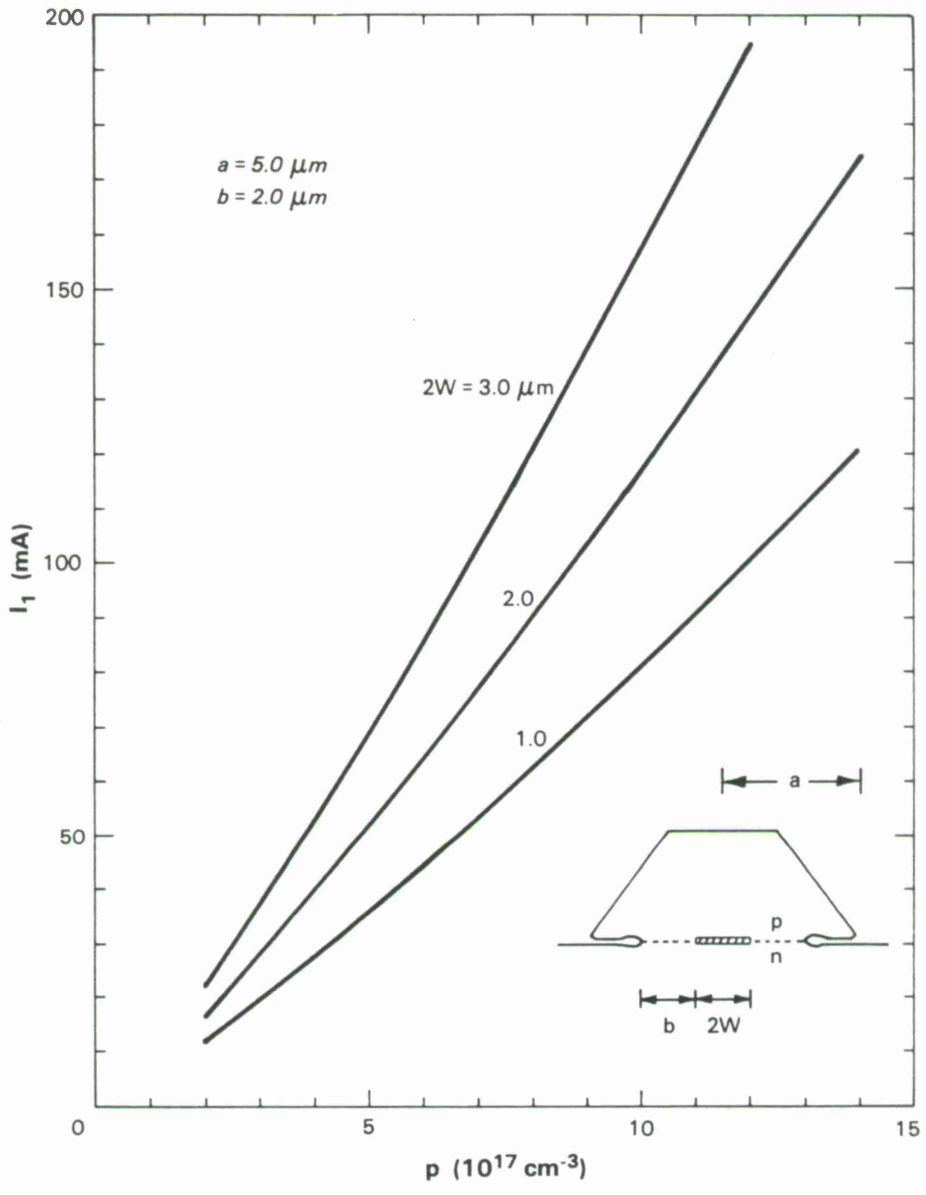


*Figure II-5. Calculated $I_1$ as a function of the cap p-doping.*

# III. LINEAR LIGHT-CURRENT CHARACTERISTICS IN MASS-TRANSPORTED GaInAsP/InP BURIED-HETEROSTRUCTURE LASERS

Linear light-output-current (L-I) characteristics and high-power operation are important for heterostructure lasers. In this work mass-transported GaInAsP/InP buried-heterostructure (BH) lasers with low threshold currents and linear light output to greater than 13 mW/facet have been obtained. This is achieved by using sufficient p-doping in the cap layer of the starting double heterostructure wafer, a technique simpler than the previously reported one (see Section I)[14] in which Zn-diffusion was employed.

Five wafers were grown with the p-doping ranging from $2.5 \times 10^{17}$ to $2.3 \times 10^{18}$ $cm^{-3}$. (The corresponding Zn concentration in the liquid-phase epitaxial growth was calibrated by using Hall-effect measurements on 8-$\mu$m-thick InP layers grown on semi-insulating substrates.) A trend of improved L-I linearity with increasing doping was observed, as shown in Figure III-1. Essentially linear characteristics up to the maximum operation current of 75 mA were obtained for wafers with $p \geqslant 9.1 \times 10^{17}$ $cm^{-3}$. Such linearity was never achieved for devices fabricated from six lightly doped wafers ($p \leqslant 3 \times 10^{17} cm^{-3}$), including the earlier ones.

However, a trend of increasing threshold current was also observed. For example, devices fabricated from wafers with $p = 9.1 \times 10^{17}$ and $2.3 \times 10^{18}$ $cm^{-3}$ showed overall threshold current increases of $\approx$50 and 200 percent, respectively, as compared with those of $p = 2.5 \times 10^{17}$ $cm^{-3}$. (The active region dimensions were presumably quite similar in these wafers.) It should be noted that increase in threshold current with the p-doping has previously been reported for broad area lasers.[9,15] In this work, an attempt to preserve the low threshold current was made by growing Wafer 635 with a thin ($\simeq 0.4$ $\mu$m) lightly doped InP layer between the active layer and the heavily doped cap ($p \simeq 7.9 \times 10^{17}$ $cm^{-3}$). This wafer resulted in threshold currents 11 to 16 mA (similar to those of light doped ones) as well as an improved L-I linearity (see the dotted curve in Figure III-1).

Figure III-2 shows far-field patterns in the junction plane. These far-field patterns are smooth compared with those of the more conventional BH lasers,[16] and single lateral mode operation was maintained up the maximum operation current of 60 mA, nearly three times the threshold current. Other devices showed a full angular width at half maximum intensity as narrow as 23°, corresponding to an active region of estimated 3-$\mu$m width and 0.15-$\mu$m thickness.

The improvement of L-I linearity with p-doping is consistent with the hypothesis of the forward-biased InP homojunctions described in Section I.[14] However, it does not rule out other possible causes such as the electron leakage over the heterobarrier.[17-19] This latter mechanism has been invoked to explain the threshold-temperature dependence in GaInAsP lasers, but its possible consequences on the L-I characteristics were not discussed.[17-19]

Z.L. Liau
J.N. Walpole
D.Z. Tsang

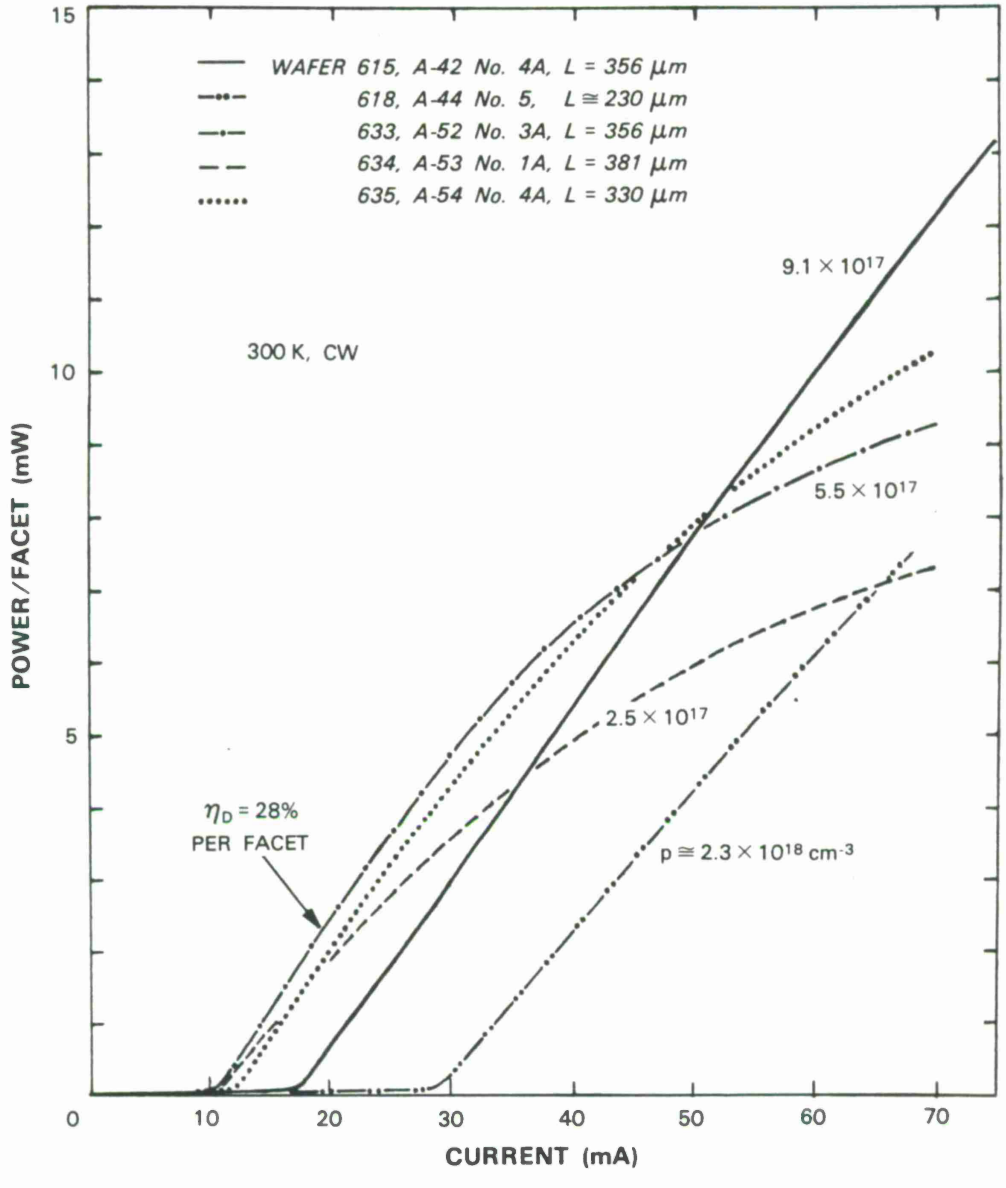


*Figure III-1. L-I characteristics of the five mass-transported BH lasers with different cap-layer doping concentrations. These devices were mounted p-side down.*

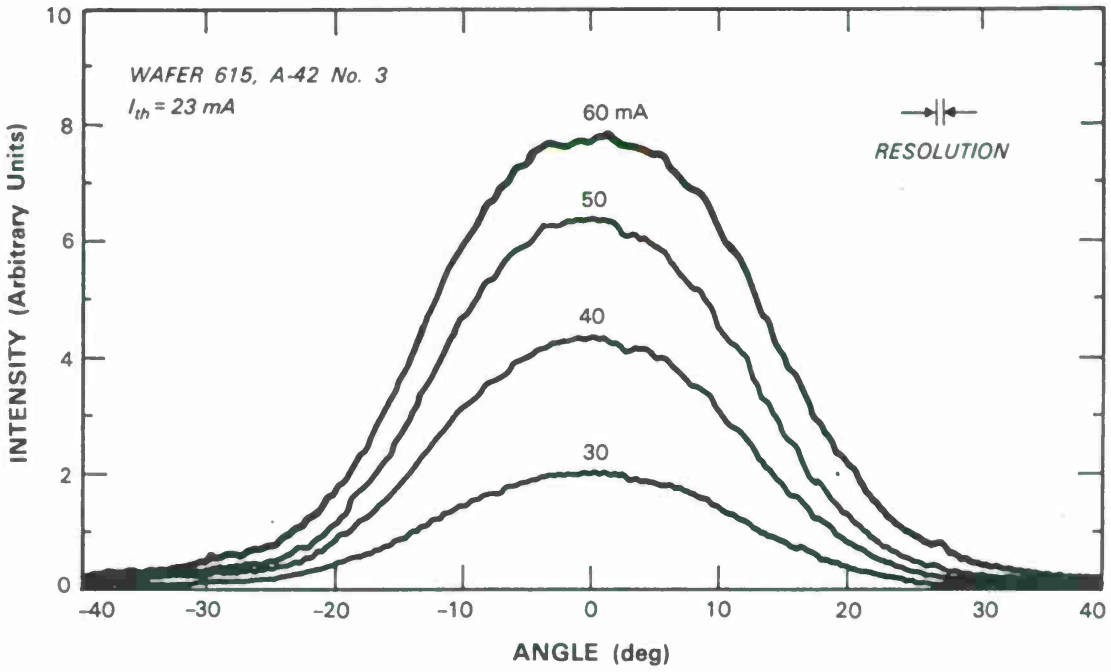


85890-10

*Figure III-2. Far-field patterns in the junction plane of a mass-transported BH laser.*

# IV. Q-SWITCHING OF LOW-THRESHOLD BURIED-HETEROSTRUCTURE DIODE LASERS AT 13 GHz

Actively Q-switched diode lasers are of interest for high-bandwidth optical fiber communication systems. Laser pulses at modulation rates of several tens of gigahertz should be possible.[20] Previously reported actively Q-switched semiconductor lasers with an integrated electroabsorption modulator have been operated on a pulsed basis with thresholds of 240 mA.[20,21] A two-section buried-heterostructure laser with a proton-isolated modulator was also reported.[22] These devices had a threshold of about 40 mA and were Q-switched at 3 GHz. Here we report buried-heterostructure Q-switched lasers[23] with thresholds as low as 14 mA at an emission wavelength of 1.3 $\mu$m. These devices are operated with dc current applied to an amplifier section and microwave modulation applied to a reverse-biased pn junction modulator. Since the capacitance of the intracavity modulator can be as low as 0.1 pF under a few volts reverse bias, the laser can be easily modulated when integrated with low-power, high-speed transistors without the high current drive required for direct-current modulation. The devices have been continuously operated with full on/off modulation confirmed at rates of 12.6 GHz.

The design, fabrication, and operation of the laser are similar to the zinc-diffused stripe Q-switched lasers reported earlier[20,21] except for modifications made to incorporate the buried heterostructure. The laser is fabricated from a double-heterostructure wafer consisting of an LPE-grown $2 \times 10^{18}$ cm$^{-3}$ Sn-doped buffer layer, a $1 \times 10^{16}$ cm$^{-3}$ n-type $Ga_{0.26}In_{0.74}As_{0.60}P_{0.40}$ active layer, and a $1 \times 10^{16}$ cm$^{-3}$ n-type InP cap layer. Both selective chemical etching to define an active region about 2-$\mu$m wide and a mass transport process[7] to bury the active region are used to form the buried heterostructure. Zinc is selectively diffused to form an amplifier section and beryllium is selectively implanted to form a modulator section, as shown in Figure IV-1. Au-Zn contacts are applied to the p-type regions and Au-Sn contacts are applied to the n-type substrate. Mirrors are formed by cleaving. The amplifier is forward-biased to produce optical gain while the modulator is reverse-biased to produce optical loss by electroabsorption (Franz-Keldysh effect). For optical energies slightly less than the band gap of the GaInAsP layer, the optical absorption can be controlled by the electric field produced in the modulator pn junction. The bulk absorption in the GaInAsP layer can be increased from a very small value to over 1000 cm$^{-1}$ as the electric field is varied from zero to $>3.6 \times 10^5$ V/cm for photon energies as much as 60 meV below the energy gap.[24] The amplifier and modulator are optically coupled but electrically isolated by the waveguide section. The cross section of the buried heterostructure is constant throughout the device. The active region is about 0.2 $\mu$m thick and 2 $\mu$m wide. The position of the beryllium-implanted junction is deliberately offset from the quaternary layer, as shown in Figure IV-1, to prevent electroabsorption at zero bias.[21] Typically the length of the amplifier is 150 to 250 $\mu$m while the length of the modulator is 25 $\mu$m.

The laser is mounted in a package between two microstriplines which bring the electrical drive signals to the two sections. In order to facilitate bonding, the device is mounted with the substrate side soldered to the heat-sink.

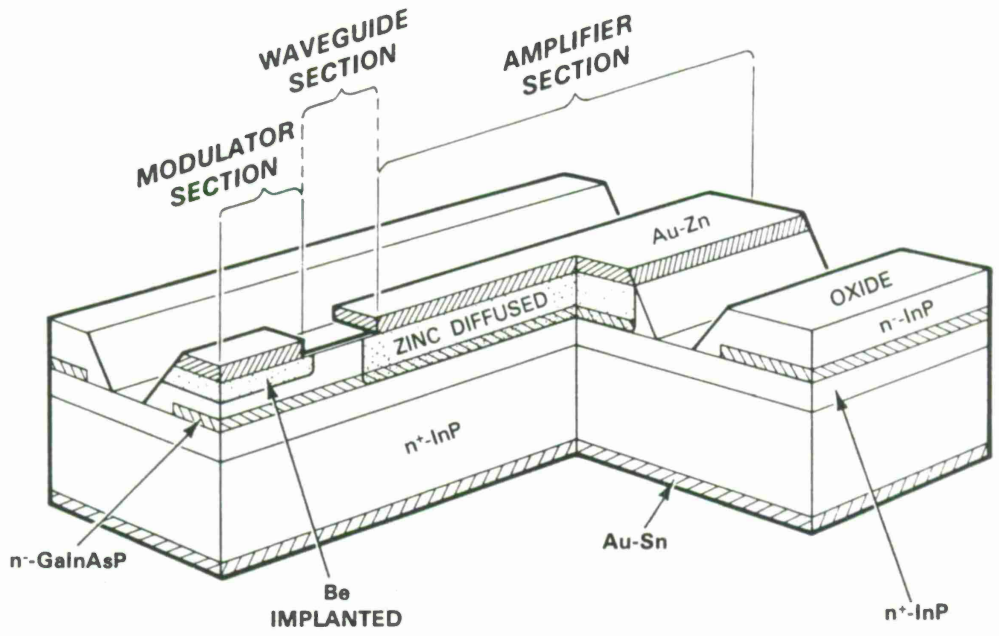


85890-11

*Figure IV-1. Perspective cutaway view of the Q-switched laser. The buried-heterostructure active region extends through all three sections of the device.*

The lasers have thresholds as low as 14 mA with the modulator open-circuited. The low threshold of the lasers permits continuous operation at room temperature. In order to characterize the modulator loss, the threshold of the laser can be measured as a function of the modulator reverse bias. At 13 V reverse bias the pulsed threshold for one device (Figure IV-2) increases by a factor of about 4.5 compared to the threshold with the modulator open-circuited, indicating a substantial variation in intracavity loss.

The devices were modulated by application of both a dc voltage and a microwave signal to the modulator.[20] Typically 70 to 200 mW of microwave power and a few volts of dc reverse bias were sufficient to drive the unmatched modulator. The devices were modulated at rates between 2 and 13.5 GHz. The optical pulses out of the laser were collected and focused on a back-illuminated 25-$\mu$m-dia. GaInAs/InP p-i-n photodiode that had <70 ps FWHM response time.[25] The detector output was displayed on a sampling oscilloscope which had a 20-ps rise time. Continuous Q-switched operation at a rate of 8 GHz with full on/off modulation is illustrated in Figure IV-3(a). The laser amplifier was driven at 2.1 times the threshold of the device with the modulator open. The modulator was dc biased with 1.3 V reverse bias. Microwave power of 100 mW was applied to the system. The actual modulator drive power was somewhat less due to insertion losses in the bias tee, cables, and connectors. Full on/off modulation was seen at 10.2 GHz as shown in Figure IV-3(b), although the detected signal is smaller. Full on/off modulation was observed up to 12.6 GHz with further reduction in output. At 13.5 GHz the depth of modulation was limited by the detector and its package.

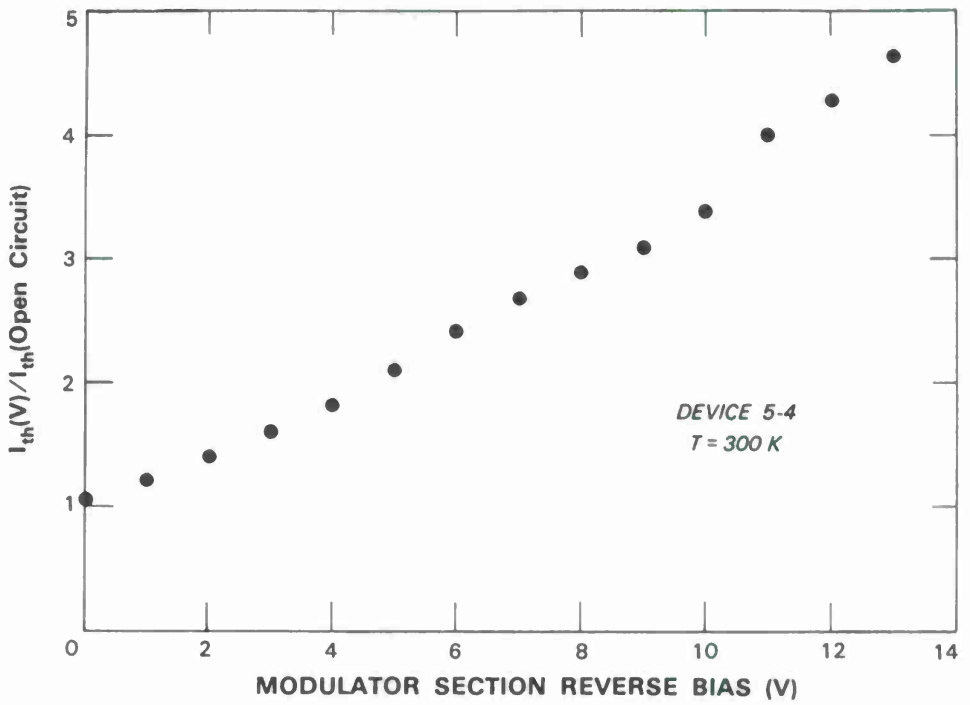


85890-12

*Figure IV-2. Pulsed threshold, normalized to the threshold of the laser with the modulator open, as a function of modulator reverse bias.*

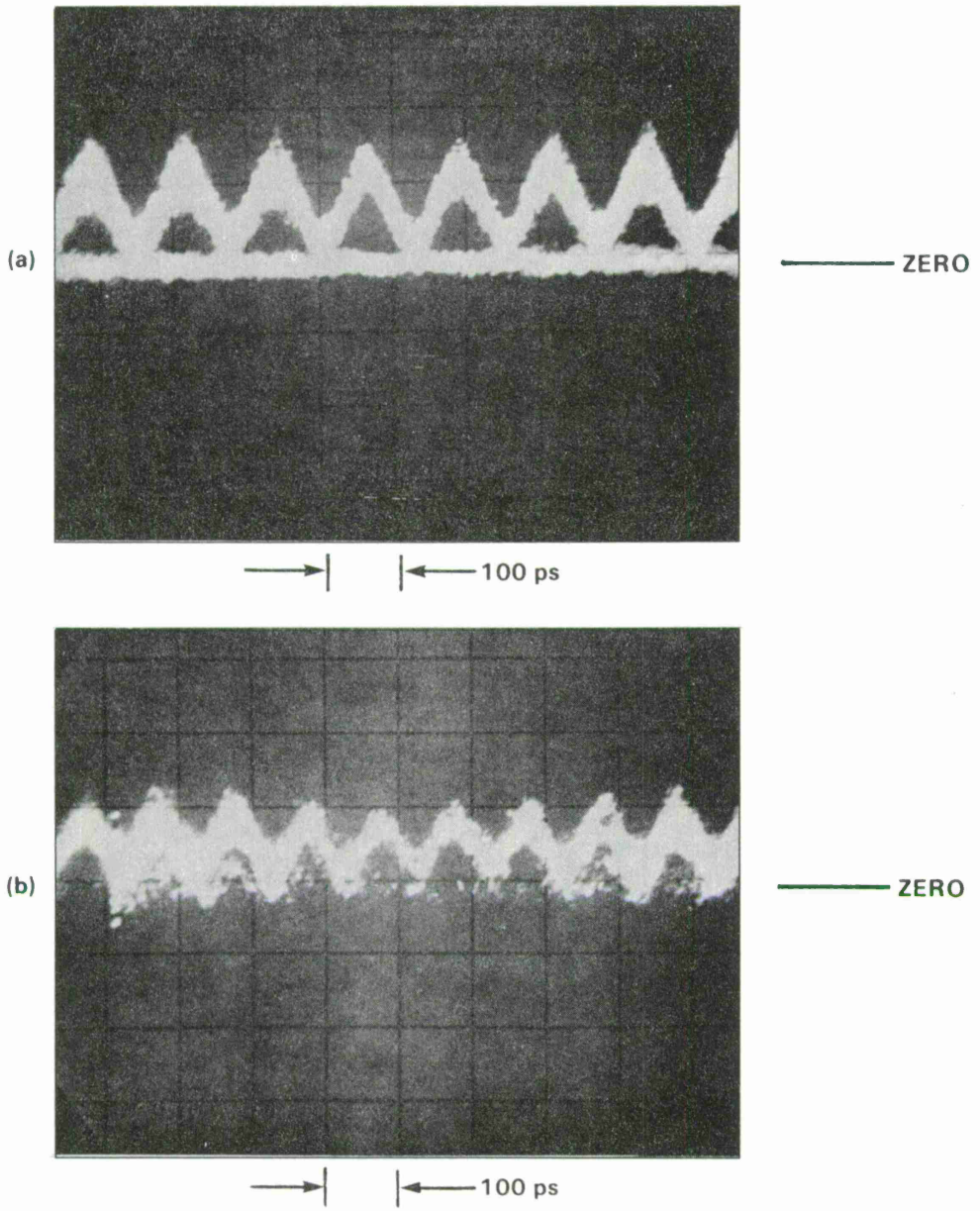


*Figure IV-3. (a) Continuous Q-switching at 8 GHz and (b) Q-switching at 10.2 GHz. Both figures have an extra trace to show the reference level with the light blocked. The intensity of the reference was reduced in (b).*

The results reported here demonstrate Q-switched diode lasers with low threshold current. The lasers have been modulated at rates above 13 GHz and should be useful for optical fiber communication systems and other applications requiring such high rates.

D.Z. Tsang
J.N. Walpole
Z.L. Liau
S.H. Groves
V. Diadiuk

# V. LOW-THRESHOLD GaInAsP/InP BURIED-HETEROSTRUCTURE LASERS WITH A CHEMICALLY ETCHED AND MASS-TRANSPORTED MIRROR

Chemically etched mirrors[26-31] are potentially very important for monolithic optoelectronic integration and for short or coupled-cavity lasers. However, the etched mirrors reported to date[26-31] were generally not flat, not vertical, or not easily applicable to the conventional buried-heterostructure lasers. These problems can be solved by using the recently developed mass-transport technique,[32] and promising initial results are described below.

Figure V-1(a) to (c) illustrates the formation of a chemically etched mirror facet and the subsequent smoothing of the facet by using the mass-transport phenomenon. The etched profile in Figure V-1(b) is obtained by a repeated use of a mixture of $H_3PO_4$ and HCl (see References 33 and 34) and an aqueous solution of $K_3Fe(CN)_6$ and KOH. The mass transport is carried out by heating the wafer at a temperature of 670° to 690°C in $H_2$ and $PH_3$ atmosphere.[32]

Figure V-2(a) and (b) shows SEM photographs of the cross sections of samples before and after the mass transport. Note that a smooth mirror surface is obtained after transport, and that the GaInAsP active region is totally buried in InP.

To fabricate the "transported mirror" on a stripe-geometry laser, we start with a mass-transported GaInAsP/InP buried-heterostructure (BH) laser wafer[32] in which the laser stripe edge is parallel to the (011) crystallographic planes; at the end of each laser mesa, a planar region is retained. The transported mirror is then formed in that planar region, as shown in the SEM perspective view of Figure V-3(a). For comparison, a BH laser mesa with a cleaved-mirror facet is shown in Figure V-3(b).

After metallization and dicing, the finished BH lasers have one transported mirror and one cleaved mirror. They are conveniently characterized by using the emission from the cleaved mirror because the transported mirror is coated during fabrication with phosphosilicate glass and Ti/Au metallization layers. A high yield of good BH lasers has been obtained. For example, 50 percent of some 40 devices tested from Wafer 657 show threshold currents between 5 and 10 mA. Figure V-4(a) and (b) shows the CW light-current characteristics and emission spectra of one device from Wafer 655 mounted p-side up.

It should be noted that the present threshold currents are significantly lower than the >50-mA values previously reported[26-29] for GaInAsP/InP lasers with etched mirrors, and are comparable to the lowest achieved for the lasers with both mirrors cleaved. Nevertheless, further improvements in threshold current, efficiency, and mode behavior might be obtained by using a better mirror coating and a shorter cavity.

Z.L. Liau
J.N. Walpole
D.Z. Tsang

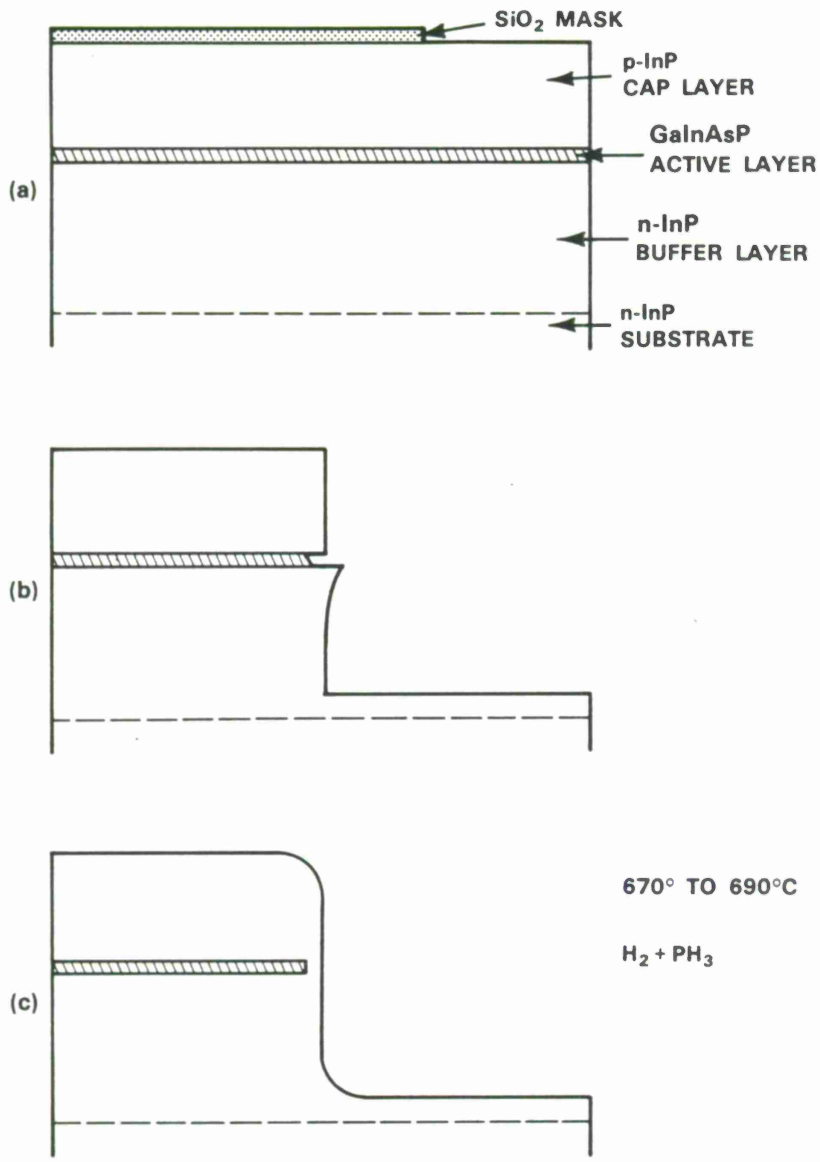


85890-14

*Figure V-1. Procedures for formation of transported mirror. The wafer was (a) initially selectively masked with oxide, (b) selectively chemical etched, and (c) mass transported.*

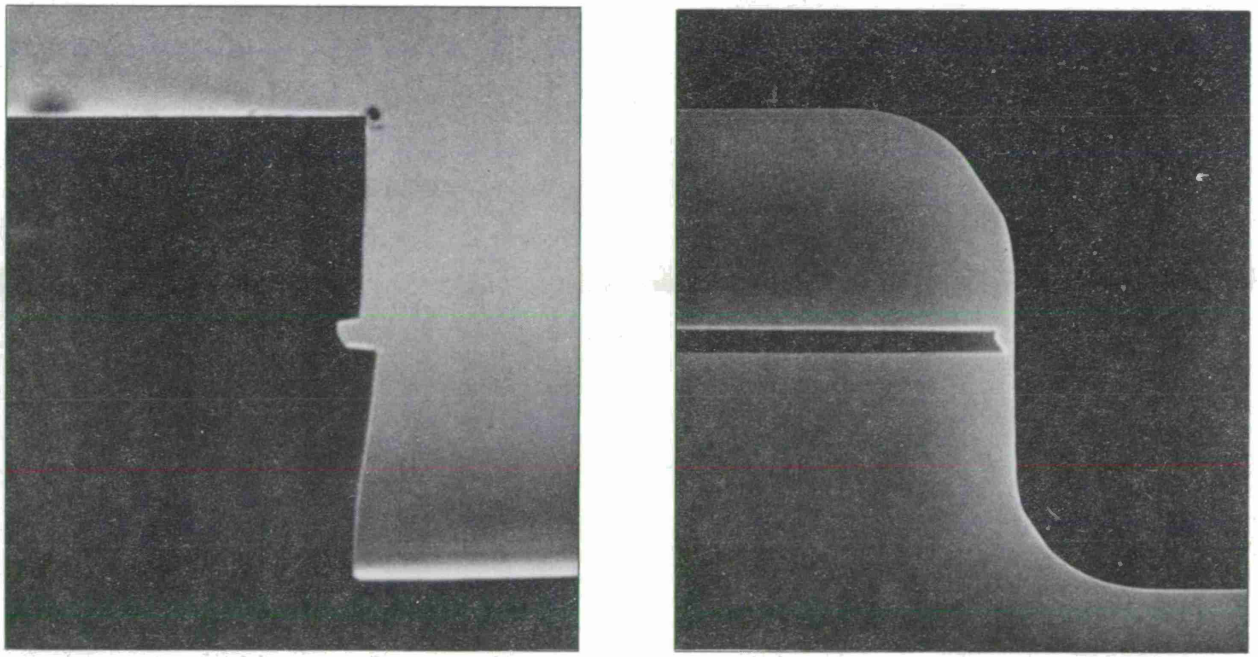


*Figure V-2. SEM photographs of longitudinal cross sections (a) before and (b) after mass transport. In (b), active layer is stained for contrast.*

(a)

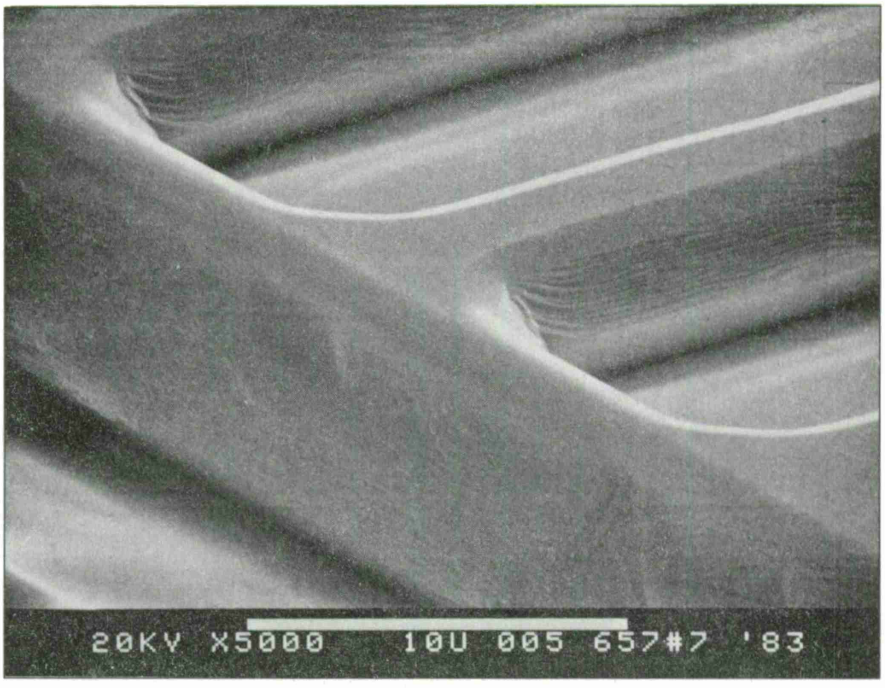


(b)

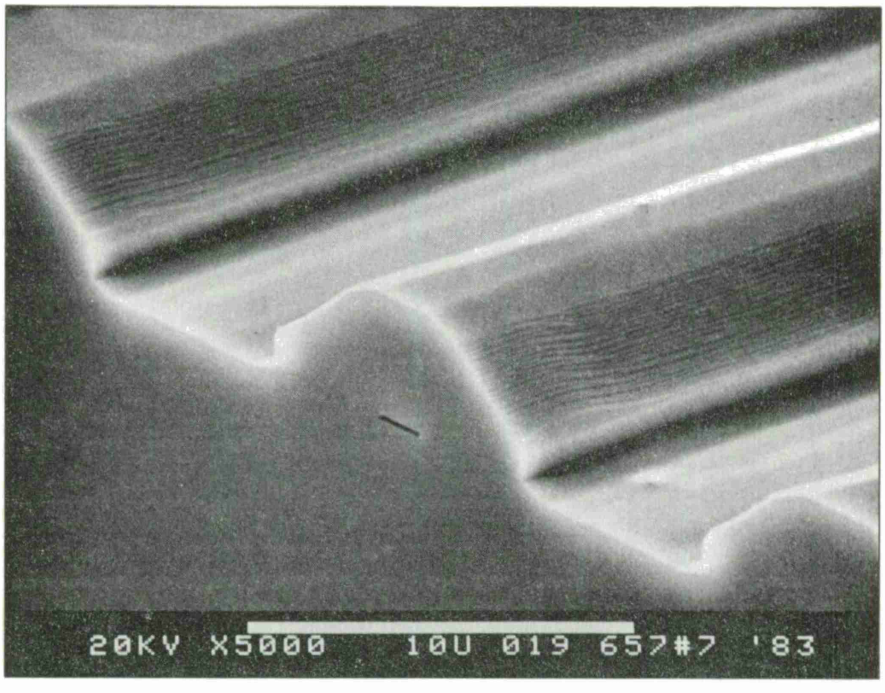


85890-16

*Figure V-3. SEM photographs showing perspective views of (a) transported and (b) cleaved mirrors. Active layer is stained for contrast.*

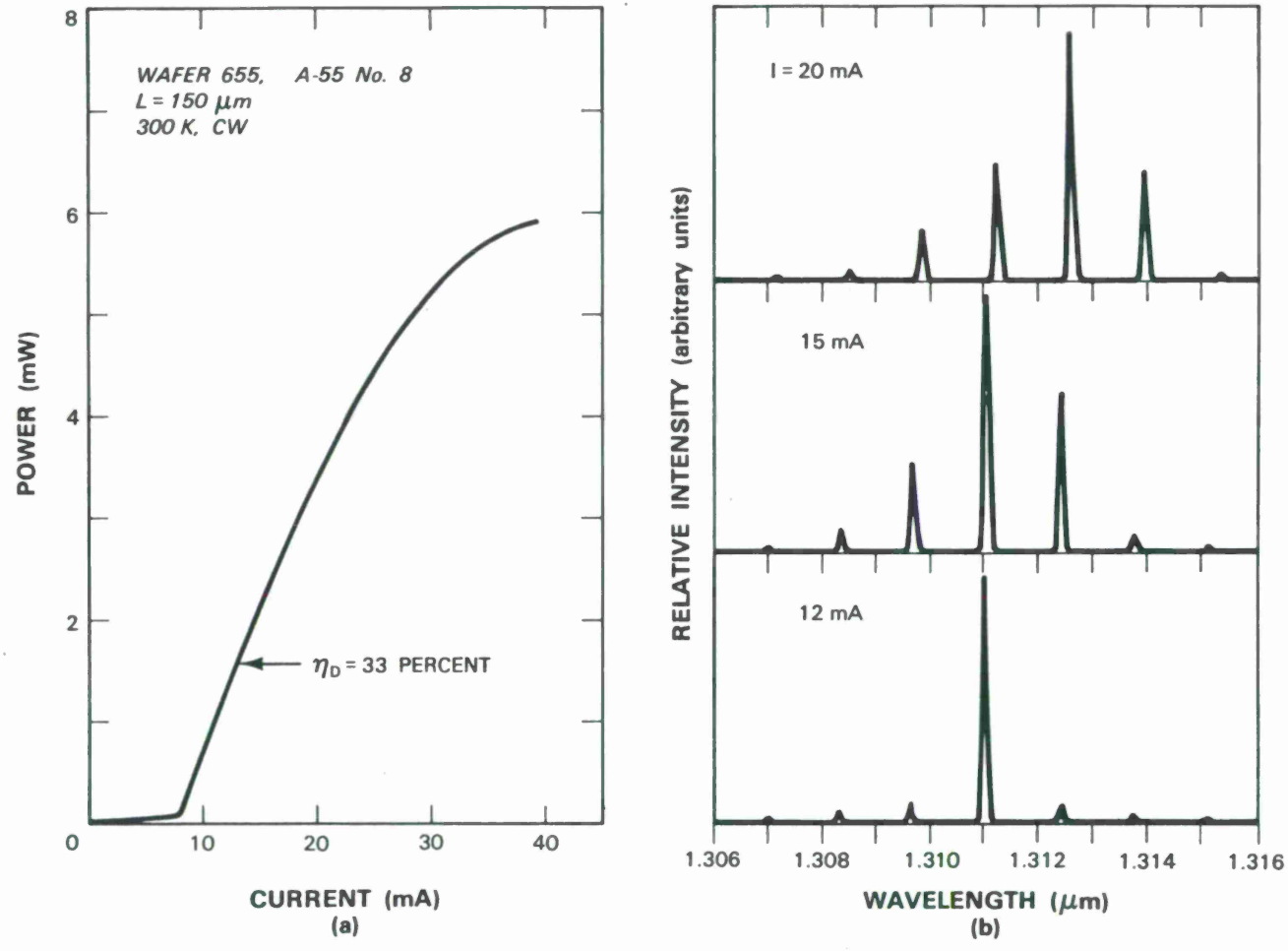


*Figure V-4. (a) Light-current characteristics and (b) emission spectra of a GaInAsP/InP BH laser with a transported mirror.*

85890-17

## REFERENCES


1. M. Hirao, A. Doi, S. Tsuji, M. Nakamura, and K. Aiki, J. Appl. Phys. **51**, 4539 (1980).
2. I. Mito, M. Kitamura, Ke. Kobayashi, and Ko. Kobayashi, Electron. Lett. **18**, 953 (1982).
3. K.L. Yu, U. Koren, T.R. Chen, and A. Yariv, IEEE J. Quantum Electron. **QE-18**, 817 (1982).
4. H. Namizaki, R. Hirano, H. Higuchi, E. Oomura, Y. Sakakibara, and W. Susaki, Electron. Lett. **18**, 703 (1982).
5. R.A. Logan, J.P. van der Ziel, H. Temkin, and C.H. Henry, *ibid.*, p. 895.
6. H. Ishikawa, H. Imai, T. Tanahashi, K. Hori, and K. Takahei, IEEE J. Quantum Electron. **QE-18**, 1704 (1982).
7. Z.L. Liau and J.N. Walpole, Appl. Phys. Lett. **40**, 568 (1982), DTIC AD-A121779; Semiannual Technical Summary "Electrooptical Devices," Lincoln Laboratory, MIT (31 March 1985).
8. Y. Itaya, Y. Suematsu, S. Katayama, K. Kishino, and S. Arai, Jpn. J. Appl. Phys. **18**, 1795 (1979).
9. W. Ng and Y.Z. Liu, Electron. Lett. **16**, 693 (1980).
10. W.R. Smythe, *Static and Dynamic Electricity*, 3rd Edition (McGraw-Hill, New York, 1968), p. 90.
11. F.B. Hildebrand, *Advanced Calculus for Applications* (Prentice-Hall, New York, 1962), p. 574.
12. N.K. Dutta, J. Appl. Phys. **51**, 6095 (1980); J. Appl. Phys. **52**, 55 (1981).
13. T.P. Pearsall, Ed;, *GaInAsP Alloy Semiconductors* (Wiley, New York, 1982), p. 308.
14. Solid State Research Report, Lincoln Laboratory, MIT (1983:1), pp. 1-5, DTIC AD-A128894/3; and Z.L. Liau, J.N. Walpole, and D.Z. Tsang, *Technical Digest*, IOOC '83 (IECE of Japan, Tokyo, 1983), p. 152.
15. Y. Itaya, Y. Suematsu, S. Katayama, K. Kishino and S. Arai, Jpn. J. Appl. Phys. **18**, 1795 (1979).
16. I. Mito, M. Kitamura, Ke. Kobayashi, S. Murata, M. Seki, Y. Odagiri, H. Nishimoto, M. Yamaguchi, and Ko. Kobayashi, IEEE J. Lightwave Technol. **LT-1**, 195 (1983).
17. P.J. Anthony and N.E. Schumaker, J. Appl. Phys. **51**, 5038 (1980).

18. C.B. Su, J. Schlafer, J. Manning, and R. Olshansky, Electron. Lett. **18**, 1108 (1982).

19. T.R. Chen, B. Chang, L.C. Chiu, K.L. Yu, S. Margalit, and A. Yariv, Appl. Phys. Lett. **43**, 217 (1983).

20. D.Z. Tsang and J.N. Walpole, IEEE J. Quantum Electron. Lett. **QE-19**, 145 (1983).

21. Semiannual Technical Summary "Electrooptical Devices," Lincoln Laboratory, MIT (30 September 1981), P. 19, and D.Z. Tsang, J.N. Walpole, S.H. Groves, J.J. Hsieh, and J.P. Donnelly, Appl. Phys. Lett. **38**, 120 (1981).

22. D.Z. Tsang, J.N. Walpole, and Z.L. Liau, IEEE Trans. Electron. Devices **ED-30**, 1596 (1983); and Solid State Research Report, Lincoln Laboratory, MIT (1983:3), p. 11.

23. D.Z. Tsang, J.N. Walpole, Z.L. Liau, and S.H. Groves, 4th Intl. Conf., Integrated Optics and Optical Fiber Communication (IOOC '83), Postdeadline Technical Digest, Tokyo, Japan, 27-30, June 1983, paper 29B5-6.

24. R.H. Kingston, Appl. Phys. Lett. **34**, 744 (1979).

25. V. Diadiuk, S.H. Groves, D.Z. Tsang, and J.N. Walpole, IEEE Trans. Electron Devices **ED-30**, 1608 (1983).

26. K. Iga and B.I. Miller, IEEE J. Quantum Electron. **QE-18**, 22 (1982), and earlier works cited therein.

27. P.D. Wright, R.J. Nelson, and R.B. Wilson, IEEE J. Quantum Electron. **QE-18**, 249 (1982), and earlier works cited therein.

28. L.A. Coldren, K. Furuya, B.I. Miller, and J.A. Rentschler, IEEE J. Quantum Electron. **QE-18**, 1679 (1982), and earlier works cited therein.

29. S. Adachi, H. Kawaguchi, K. Takahei, and Y. Noguchi, J. Appl. Phys. **52**, 5843 (1981).

30. K. Furuya, L.A. Coldren, and B.I. Miller, J.A. Rentschler, Electron. Lett. **17**, 582 (1981).

31. L.A. Coldren, K. Furuya, and B.I. Miller, J. Electrochem. Soc. **130**, 1918 (1983).

32. Z.L. Liau and J.N. Walpole, Appl. Phys. Lett. **40**, 568 (1982), DTIC AD-A121779.

33. Solid State Research Report, Lincoln Laboratory, MIT (1984:2), DTIC AD-A147640, p. 3; also J.P. Donnelly, N.L. DeMeo, G.A. Ferrante, K.B. Nichols, and F.J. O'Donnell, Appl. Phys. Lett. **45**, 360 (1984).

34. K. Iwasaki, S. Kurazano, and K. Itakuma, Electron Commun. Jpn. **58-C**, 100 (1975).

# APPENDIX A

# Fabrication, Characterization, and Analysis of Mass-Transported GaInAsP/InP Buried-Heterostructure Lasers

Z. L. LIAU, JAMES N. WALPOLE, AND DEAN Z. TSANG, MEMBER, IEEE

*Abstract*—The mass-transported buried-heterostructure lasers have been investigated in detail. Techniques have been developed for fabrication control and wafer characterization. High yield of low-threshold lasers was obtained with the lowest threshold current being 5.5 mA. Differential quantum efficiencies as high as 28 percent per facet and smooth far-field patterns were also obtained. Deep Zn-diffusion and higher p-doping have been used to improve the linearity of the light-current characteristics. Linear light output to greater than 13 mW per facet and well-behaved threshold-temperature dependence were achieved. A conformal mapping technique has been used to calculate the voltage distribution in the laser mesa. The forward-bias voltage thus obtained for the InP pn homojunctions in the transported regions is shown to be capable of resulting in the sublinear dependence of light output on current observed in lasers with lightly p-doped cap layers. The current limit within which the laser can be operated without leakage through the homojunctions has been calculated for various device geometries and doping levels.

## I. Introduction

GaInAsP/InP buried-heterostructure (BH) lasers are among the most important light sources for fiber optic communications and integrated optics. In recent years, considerable effort has been devoted to the development of these lasers and excellent device characteristics have been obtained [1]-[16]. Recently, a new fabrication technique based on a mass-transport phenomenon was reported [17]-[26]. It has unique capabilities, is simpler compared to the more conventional fabrication techniques and has resulted in BH lasers with low threshold currents [17]-[20].

For a more complete evaluation of the new technique, we have carried out in this work a detailed investigation. First, supporting and reference mesas have been introduced for the mechanical protection of the laser mesa and for improved fabrication control, respectively, and have resulted in high device yield. Second, the laser mesa and its uniformity and smoothness have been better characterized for optimum device performance. Third, the device characteristics have been studied in detail with a special emphasis on linear light output at high powers. Finally, a theoretical analysis has been carried out to aid in eliminating current leakage through the InP p-n homojunctions in the transported regions.

## II. Experimental Procedure

The fabrication starts with double heterostructure wafers grown by conventional liquid-phase epitaxy (LPE). Each wafer consists of three layers grown on a Sn-doped (100) InP substrate: 1) a Sn-doped ($n = 2 \times 10^{18}$ cm$^{-3}$, unless otherwise stated) InP buffer layer of 3-4 $\mu$m thickness, 2) a nominally undoped $Ga_{0.27}In_{0.73}As_{0.63}P_{0.37}$ active layer [27] with a thickness of 0.15-0.25 $\mu$m and 3) a Zn-doped cap layer of 2-3.5 $\mu$m thickness. Various atomic fractions of Zn, $X^l_{Zn}$ of $1.0\text{-}7.3 \times 10^{-5}$, have been used in the cap layer growth solutions in growing different wafers.

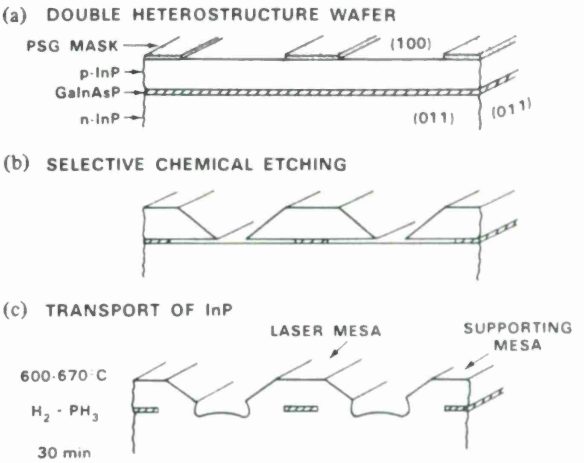


Fig. 1. Schematic pictures showing the mass-transported BH technique.

A phosphosilicate glass (PSG) layer approximately 500 Å thick is first deposited on each wafer. Pairs of stripe openings are formed on the PSG using photolithographic techniques as illustrated in Fig. 1(a). A sequence of three chemical etching steps is then carried out to form the mesa structure shown in Fig. 1(b). First, either HCl or Br-methanol is used to etch the regions not protected by the PSG mask. Br-methanol has been used in the latest runs (since Wafer 602) [28]. For this etchant the PSG stripe edges are always made parallel to the (011) planes [29], [30]. The same PSG stripe direction is also preferred for HCl etching because of easier control. (For results presented in this paper only Wafer 513 of Fig. 4 was etched using HCl with stripes parallel to the $(01\bar{1})$ planes.) Second, the PSG stripe mask is removed by using buffer-HF and the wafer is cleaned. Finally, an aqueous solution of $K_3Fe(CN)_6$ and KOH is used to etch the quaternary active layer to the desired width [17]. Quaternary widths 0.5-3.0 $\mu$m are routinely obtained by using the reference mesas [17], [20] for etching control as illustrated in Fig. 2.

The mass transport is carried out by loading the wafer into a conventional LPE system, but without any growth solution [17]. The system is purged with $PH_3$ and purified $H_2$ and

Manuscript received January 9, 1984. This work was supported by the U.S. Department of the Air Force.

The authors are with the Lincoln Laboratory, Massachusetts Institute of Technology, Lexington, MA 02173.

0018-9197/84/0800-0855$01.00 © 1984 IEEE

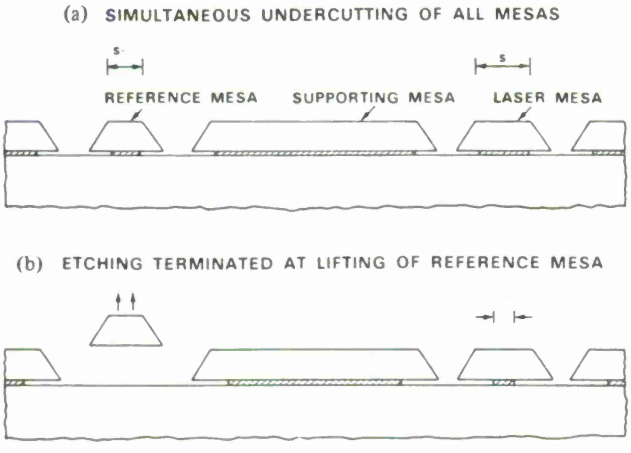


Fig. 2. A technique for controlling the quaternary region width during the selective chemical etching. The reference mesa was made slightly narrower than the laser mesa in order to signal for the termination of the etching [17], [20].

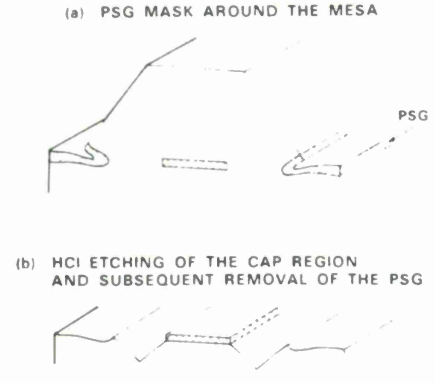


Fig. 3. A technique to expose the quaternary active region for examination. The cap region was selectively etched away by using HCl and the PSG mask was subsequently removed.

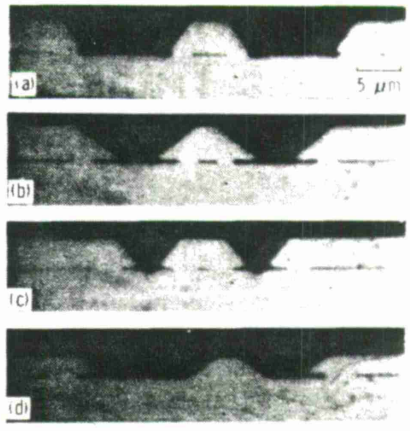


Fig. 4. Optical micrographs of various types of mass-transported BH mesas. Samples in (a), (b), (c), and (d) were from Wafers 513, 514, 635, and 522, respectively.

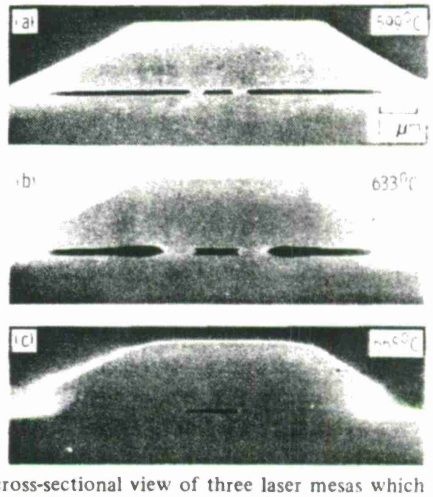


Fig. 5. SEM cross-sectional view of three laser mesas which have been transported at different temperatures. Samples in (a), (b), and (c) were from Wafers 549, 553, and 528, respectively.

heated to a temperature of 600-670°C in 30 min. It is then kept at the steady state temperature for another 30 min before being rapidly cooled down.

After the mass transport, one or more bars are cleaved off the wafer for the examination of the mesa cross sections. To delineate the quaternary region or junctions in the InP, the cleaved facets are stained in solutions similar to the quaternary etch mentioned in the previous paragraph. To characterize the active regions over the entire wafer, additional examination was carried out for some wafers on the exposed quaternary and transported regions by removing the cap as illustrated in Fig. 3.

Most of the mass-transported wafers are processed into BH lasers by using the procedure described previously [17]. For some wafers, processing involved an additional Zn-diffusion to a depth of 1-2 μm over the entire wafer [20]. This deep Zn-diffusion was carried out by loading the wafer into a sealed quartz ampoule along with some zinc-phosphide and InP powders and by heating to 450°C for 160-190 min followed by a short diffusion at 600°C for 2 min. This latter diffusion helps reduce contact resistance.

## III. Results and Discussion

Fig. 4(a), (b) shows stained cross sections of mass-transported BH mesas for which HCl was used in the mesa etching with stripe edges parallel to $(01\bar{1})$ and (011) planes, respectively. Note that mesa angles characteristic of HCl etching along the two different crystallographic directions [5], [30] are seen. Shown in Fig. 4(c) is a BH mesa for which Br-methanol was used in the etching. These figures show that BH lasers with desired active region widths can be fabricated along any crystallographic direction by using the mass-transport technique. This evidently provides greater flexibility in device design (e.g., fabrication of chemically etched mirrors [30]), as compared to the more conventional BH techniques [1]-[16] which are virtually limited to the stripe direction parallel to the $(01\bar{1})$ planes. Fig. 4(d) shows a phenomenon often observed for the reference mesas (cf. Fig. 2), in which the mesa was totally undercut, deflected away from its original central position, but was subsequently fused back onto the wafer by the mass transport.

The scanning electron microscope (SEM) photographs in Fig. 5 show an increase of transported region with temperature. At a given temperature, the width of the transported region is

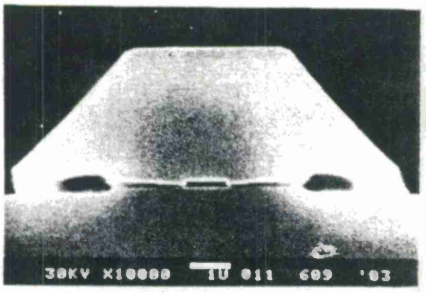


Fig. 6. SEM cross-sectional view of a laser mesa showing the formation of InP p-n homojunctions in the transported regions. The steps seen in the transported regions are due to the staining procedure which preferentially eroded n-InP as confirmed by rotating the sample during the SEM examination. The sample was from Wafer 609 whose buffer layer was doped to $n \simeq 1 \times 10^{18}$ cm$^{-3}$.

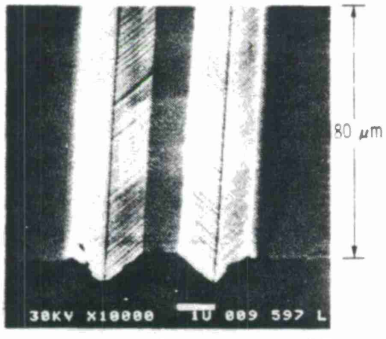


Fig. 7. SEM perspective view of a laser mesa (of Wafer 597) after the cap has been removed by HCl etching (cf. Fig. 3).

approximately inversely proportional to the active layer thickness. A fixed transport temperature of 650°C has been used since Wafer 584 and transported region widths of approximately 2.0 μm are obtained for active layer thicknesses of approximately 0.15 μm.

Fig. 6 shows the SEM photograph of a cleaved laser mesa which has been stained to reveal junctions in InP. Formation of pn homojunctions in the transported InP regions is seen.

Fig. 7 shows an SEM photograph of the perspective view of an exposed quaternary active region (cf. Fig. 3) which is 1.0 μm in width. The photograph shows 80 μm of the stripe length, because the wafer was tilted at a glancing angle during the SEM examination. Some roughness (≤500 Å) is seen along the edges of the quaternary region. This roughness is believed to have originated from the PSG mask, because a very similar roughness was also observed on the sidewalls of the laser mesas. The active region width varies gradually within a wafer, with a range of variation of ±1 μm about the average value. This variation is attributed to variations in cap layer thickness, in PSG stripe width and perhaps also in the active layer thickness. Transported region width as uniform as ±10 percent over the entire wafer has been observed.

High yield of low-threshold lasers has been obtained. Fig. 8 shows statistics of pulsed threshold currents of devices fabricated from a single wafer. This wafer has active region widths of 1.1-1.9 μm (measured on a cleaved bar) and transported region width of 0.4 μm, and 80 percent of 130 devices tested show threshold currents of 10-30 mA. Similar low-threshold currents have been obtained for lasers fabricated parallel to either (011) or (01$\bar{1}$) planes, by using either HCl or Br-methanol for mesa etching, and with temperatures of 608-670°C for mass transport. The lowest threshold current obtained to date is 5.5 mA (from Wafer 514). A fraction of the devices (normally those with lower thresholds) are mounted on copper heat sinks for CW operation. It is worth mentioning that filling of indium solder into the grooves between laser and supporting mesas has been observed, when the device is soldered p-side down to the heat sink. After mounting, the increases in threshold current were generally less than 3 mA. Fig. 9 shows the light-current ($L$-$I$) characteristics of a device from Wafer 514. This device is mounted p-side up and shows a threshold current of 7.5 mA (same as the pulsed) with an initial differential quantum efficiency $\eta_D$ of 20 percent per facet.

In an effort to obtain high $\eta_D$, wider active region width (1.5-3.5 μm within each wafer) and improved stripe smoothness have been used (since Wafer 591) in order to minimize the sidewall scattering loss [31]. Differential quantum efficiencies of 20-25 percent per facet have been reproducibly obtained with the highest being 28 percent per facet. Still higher $\eta_D$ may be obtained with thinner and wider active regions and shorter devices.

All devices fabricated from earlier wafers (before Wafer 584), however, showed sublinear $L$-$I$ characteristics shortly after reaching threshold, as evident in Fig. 9. Severer sublinearity was observed at higher currents. This effect can be explained by current leakage through the InP p-n homojunctions. Consider the current flowing from the ohmic contact on top of a laser mesa such as that in Fig. 6. When the current is relatively low, it flows predominantly through the active region, with only a negligibly small portion flowing through the InP p-n homojunctions, because the quaternary has an energy gap smaller than that of InP. However, a portion of the current will flow laterally (i.e., along the InP p-n homojunctions) to reach the active region. Thus, the voltage needed to drive the current also forward-biases the homojunctions, especially in the regions upstream of the current flow. This forward bias increases with the current, eventually turns on the homojunctions and can therefore lead to the sublinear $L$-$I$ characteristics. (For a more rigorous treatment of this problem, see Section IV.)

The voltage increase is predominantly on the p-side, because its resistivity is significantly higher than that of the n-side. (The p-type cap layer is relatively lightly doped compared to the n-type buffer layer and holes have considerably lower mobility than electrons.) The [illegible]ation can therefore be significantly improved by using highe[illegible] p-doping. For this purpose, Zn-doping in the LPE growth was investigated. Hall effect measurements on 8-μm-thick InP layers grown on semiinsulating InP substrates by using $X_{Zn}^{l}$ of 3.0, 5.0, and 7.0 × 10$^{-5}$ showed hole concentrations of 0.92, 1.53, and 2.25 × 10$^{18}$ cm$^{-3}$, respectively, and Hall mobilities of 70-100 cm$^2$/V · s. Nominally undoped InP layers showed background n-type dopings of approximately 1 × 10$^{17}$ cm$^{-3}$. These results suggest that hole concentrations are no greater than 3 × 10$^{17}$ cm$^{-3}$ in our earlier wafers for which $X_{Zn}^{l} \leq 1.2 \times 10^{-5}$ was used. This low p-doping was initially chosen because higher p-doping had been known to greatly increase the laser threshold [32], [33].

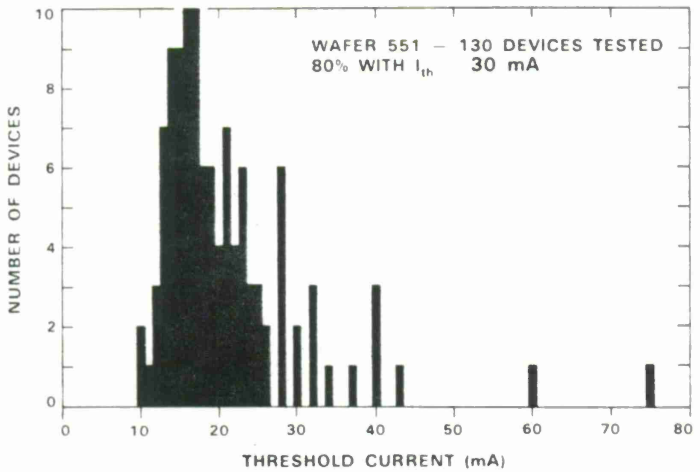


Fig. 8. Statistics of threshold currents for all devices fabricated from one mass-transported BH wafer.

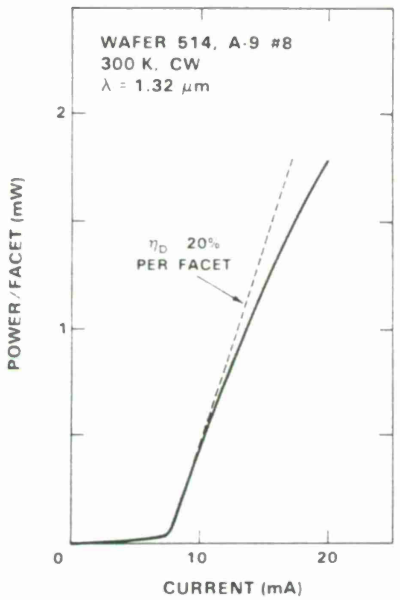


Fig. 9. The *L-I* characteristics of a mass-transported BH laser.

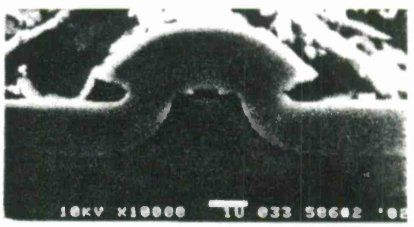

Fig. 10. SEM photograph of a stained cross section of a laser mesa which has been deep Zn-diffused over the entire wafer. This sample was from Wafer 586 whose buffer layer was doped to $n \simeq 1 \times 10^{18}$ cm$^{-3}$.

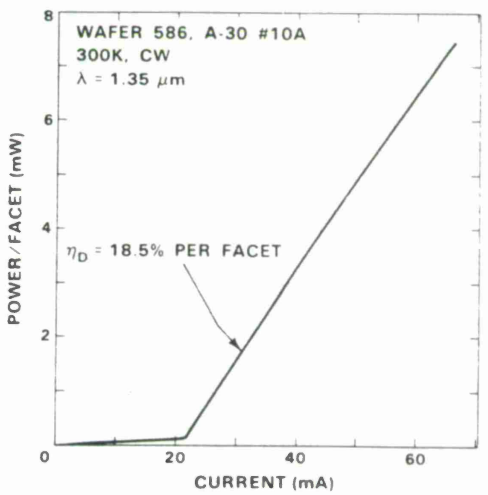


Fig. 11. The *L-I* characteristics of a mass-transported BH laser with the deep Zn diffusion. This device was mounted p-side down.

To improve the *L-I* linearity, deep Zn-diffusion was first used to increase the p-doping in the cap region [20]. An SEM photograph of a cleaved stained cross section is shown in Fig. 10. Note that the deep Zn-diffusion relocates most of the InP homojunction downward to region of lower voltage. Nevertheless, the diffusion is so designed that a lightly doped region is retained near the quaternary in order to avoid a large increase in threshold current. Wafers 584 and 586 were thus diffused to depths of 1.1 and 1.45 μm, respectively, and indeed resulted in significant improvement of *L-I* linearity, as shown in Fig. 11.

Zn-diffusion depths 1.5 to 2.0 μm are desired for optimum device design. Attempts to diffuse to these depths, however, resulted in an "enhanced diffusion" near the quaternary region, as shown in Fig. 12. This enhancement pushes the p-n junction near the quaternary region into the buffer layer by 0.6 μm, but leaves the adjacent InP p-n homojunctions virtually unmoved. In addition, several Zn diffusions were carried out with part of the wafer coated with PSG and the "enhanced diffusion" was observed only in the uncoated regions.

Another technique investigated to improve the *L-I* linearity is to dope the p-InP cap layer more heavily in the LPE growth of the starting double heterostructure wafer. For this purpose, five wafers were grown with the p-doping ranging from $2.5 \times 10^{17}$ to $2.3 \times 10^{18}$ cm$^{-3}$. A trend of improved *L-I* linearity with increasing doping has been observed as shown in Fig. 13.

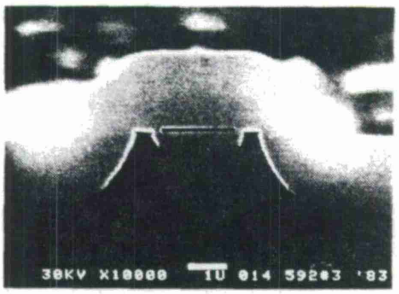


Fig. 12. SEM photograph of the stained cross section of a laser mesa which has been deep Zn-diffused and shows an "enhanced diffusion" near the quaternary active region. This sample was from Wafer 592 whose buffer layer was doped to $n \simeq 1 \times 10^{17}$ cm$^{-3}$.

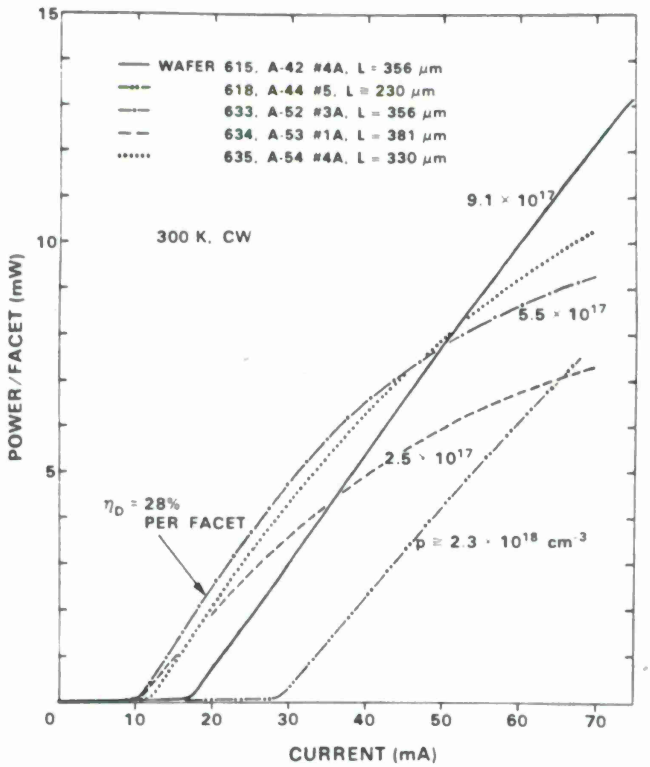


Fig. 13. *L-I* characteristics of five mass-transported BH lasers with different cap-layer doping concentrations. These devices were mounted p-side down.

Essentially linear characteristics up to the maximum operation current of 75 mA have been obtained for wafers with $p \geq 9.1 \times 10^{17}$ cm$^{-3}$. Such linearity was never achieved for devices fabricated from six other lightly doped wafers with $p \leq 3 \times 10^{17}$ cm$^{-3}$.

However, a trend of increasing threshold current has also been observed. For example, devices fabricated from wafers with $p$ of $9.1 \times 10^{17}$ and $2.3 \times 10^{18}$ cm$^{-3}$ showed overall threshold current increases of approximately 50 and 200 percent, respectively, as compared to those with $p$ of $2.5 \times 10^{17}$ cm$^{-3}$. (The active region dimensions were presumably quite similar in these wafers.) An attempt to preserve the low-threshold current was made by growing Wafer 635 with a thin (approximately 0.4 μm) lightly doped InP layer between the active layer and the heavily doped cap ($p \simeq 7.9 \times 10^{17}$ cm$^{-3}$). This wafer

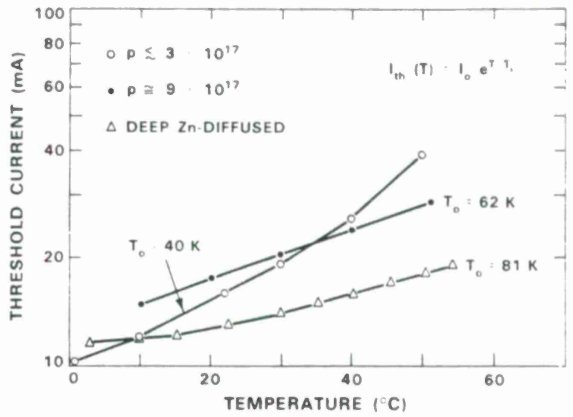


Fig. 14. Pulsed threshold current versus temperature plots of three mass-transported BH lasers. These devices are from Wafers 513(0), 615(0), and 584(Δ).

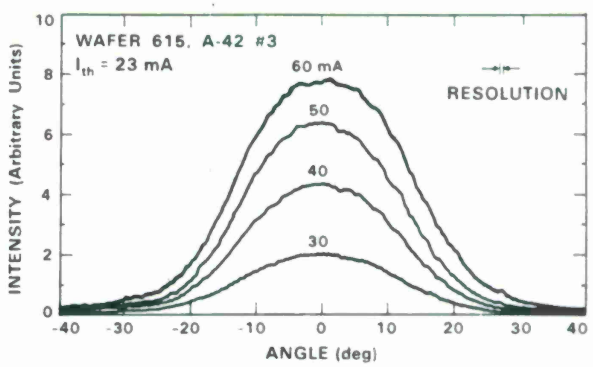


Fig. 15. Far-field patterns in the junction plane of a mass-transported BH laser.

resulted in threshold currents of 11-16 mA (similar to those of lightly doped ones) as well as an improved *L-I* linearity. (See the dotted curve in Fig. 13.)

The improvement of *L-I* linearity with p-doping is consistent with the hypothesis of the forward-biased InP homojunctions described in a previous paragraph. However, it does not rule out other possible causes such as the electron leakage over the heterobarrier [34]-[36]. This latter mechanism has been invoked to explain the threshold-temperature dependence in GaInAsP lasers but its possible consequences on the *L-I* characteristics were not discussed [34]-[36].

Fig. 14 shows some examples of the temperature dependence of the threshold current. The low $T_o$ (40 K at room temperature) of the lightly doped wafer is possibly related to the current loss through the InP homojunctions. On the other hand, $T_o$'s in the 70's were obtained for Wafer 618 ($p \simeq 2.3 \times 10^{18}$ cm$^{-3}$, not shown in Fig. 14) and those in the 80's were obtained for deep Zn-diffused wafers. It should be noted that Mito *et al.* [15] have reported that $T_o$ increases with the cap-layer p-doping.

Fig. 15 shows far-field patterns in the junction plane of a laser with a good *L-I* linearity. These far-field patterns are smooth compared to those of the more conventional BH lasers [15], and single lateral mode operation is maintained up to the maximum operation current of 60 mA, nearly three times

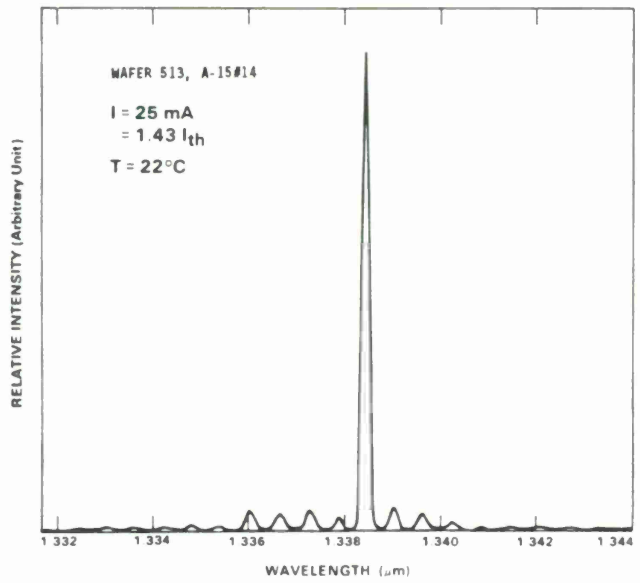


Fig. 16. Emission spectrum of a mass-transported BH laser.

the threshold current. Other devices show a full angular width at half maximum intensity as narrow as 23°, corresponding to an active region of estimated 3 μm width and 0.15 μm thickness.

Most emission spectra show multiple longitudinal mode operation (typically 5 modes). Some devices show predominantly single longitudinal mode operation within certain current ranges, as shown in Fig. 16.

## IV. Theory of Voltage and Current Distributions in the Laser Mesa

To prevent the current from flowing through the InP pn homojunctions is a matter of basic importance in the present laser structure. For this purpose, a theoretical analysis has been carried out and will be described in this section.

Consider the current flowing from the ohmic contact on top of a laser mesa such as that shown in Fig. 6. When the current is relatively low, it flows predominantly through the active region, as discussed in a previous paragraph. This current-flow pattern and the corresponding voltage distribution in the laser mesa are analyzed by using a conformal mapping technique, the Schwarz-Christoffel transformation. The forward bias voltages along the InP p-n homojunctions are obtained from this analysis and can be used to check if the homojunction current indeed remains negligibly small. Thus, the present calculation scheme is valuable in predicting the current limit within which the laser can be operated without leakage through the homojunctions.

As illustrated in Figs. 17 and 18, the cross section of the laser mesa is approximated as a trapezoidal region with base angles ($\alpha$) of 0.927 radian (53°, cf. Figs. 4 and 6) in the upper complex $w$-plane ($w = u + iv$). The active region is approximated as an equipotential line segment (from $w = -W$ to $w = W$). Another equipotential is near the ohmic contact on the mesa top. In addition, no current is allowed to flow across the mesa sidewalls and the InP p-n homojunctions. These boundary conditions are to be satisfied by the potential $\Phi(u, v)$. The latter

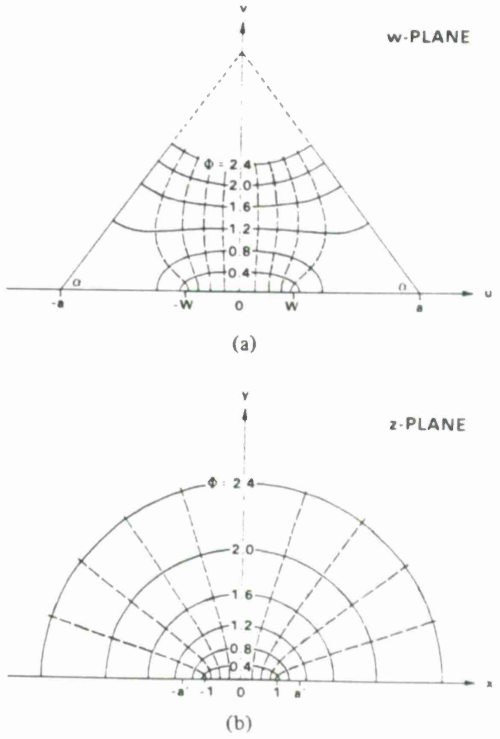


Fig. 17. The Schwarz-Christoffel transformation used to obtain the potential $\Phi(u, v)$ in the laser mesa. The dashed curves are the streamlines.

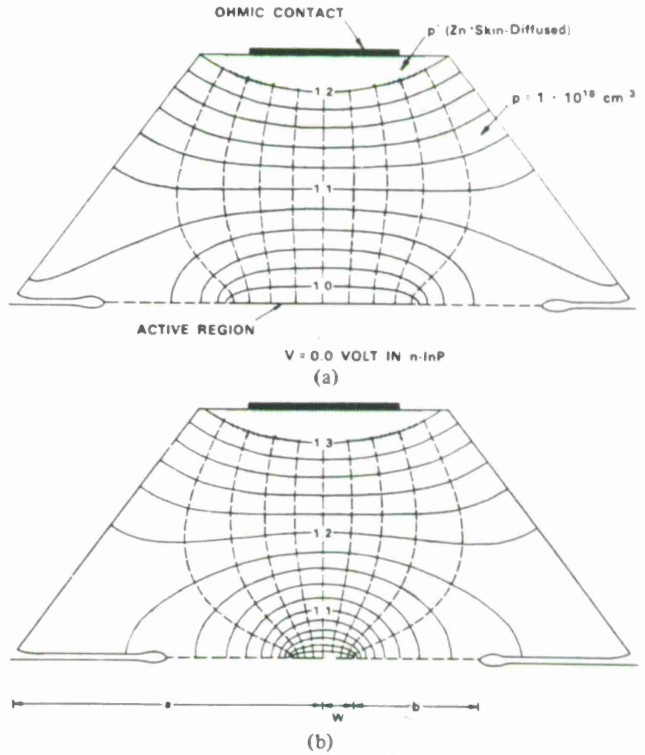


Fig. 18. Calculated voltage distribution for two laser mesas with different active region widths. The equipotentials are separated by equal voltage increments with the numbers labeling the voltage values in volts. The dashed curves are the streamlines. In these calculations and others to follow, $L$ = 300 μm and $\rho = (pq\mu_p)^{-1}$ with $\mu_p$ = 70 cm²/(V · s) were used. (a) $2W$ = 3.0 μm, $a$ = 5.0 μm, $I_Q$ = 100 mA. (b) $2W$ = 1.0 μm.

is obtained by transforming a known potential $\Phi(x, y)$ from the upper complex $z$-plane ($z = x + iy$).

The potential $\Phi(x, y)$ in Fig. 17(b) is that of a two-dimensional current flow from infinity into a slit opening [37], [38] which has a width from $z = -1$ to $z = 1$ and is maintained at a constant potential of $\Phi = 0$. The equipotentials are confocal ellipses, with foci at $z = -1$ and $z = 1$, and are given by

$$\frac{x^2}{\cosh^2 \Phi} + \frac{y^2}{\sinh^2 \Phi} = 1. \tag{1}$$

The upper complex $z$-plane is transformed into the triangular region in the upper complex $w$-plane in Fig. 17(a) by [37], [38]

$$w = K \int_0^z (z' + a')^{\alpha/\pi - 1} (z' - a')^{\alpha/\pi - 1}\, dz' \tag{2}$$

where $K$ and $a'$ are constants and are determined by requiring the mapping of $z = 1$ and $a'$ to $w = W$ and $a$, respectively, and where $\alpha = 0.927$ rad as mentioned above.

By evaluating (1) and (2) numerically, $\Phi(u, v)$ is obtained (cf. Appendix A). Some examples are shown in Figs. 17(a) and 18. (The equipotentials in Fig. 18 are labeled in $V$ which can be related to $\Phi$ as discussed below.) Note the equipotentials near the mesa tops are curved and one of them will approximately coincide with the front of the Zn-skin-diffused $p^+$ region [17], as illustrated in Fig. 18. The lateral current flow and the resulting forward bias on the InP homojunctions can be clearly visualized in these calculated current-flow patterns, especially the one with narrow active region in Fig. 18(b).

The potential $\Phi(u, v)$ is converted into the voltage distribution $V(u, v)$ by

$$V(u, v) = \frac{\rho I_Q}{\pi L}\, \Phi(u, v) + V_Q \tag{3}$$

where $\rho$ and $L$ are the resistivity and device length, respectively, and $I_Q$ and $V_Q$ are the current flowing through and the junction voltage at the quaternary region, respectively. Equation (3) is obtained by letting $V(u, v) = \text{constant} \times \Phi(u, v) + V_Q$ and by requiring $L/\rho \int_{-W}^{W} [\partial V/\partial v]_{v=o}\, du = I_Q$.

The junction voltage $V_Q$ is given by $V_Q = (F_c - F_v)/q$, where $F_c$ and $F_v$ are the quasi-Fermi levels in the conduction and valence bands of the quaternary, respectively, and $q$ is the electronic charge. Assuming parabolic energy bands with effective masses of 0.059 and 0.486 times the free electron mass in the conduction and valence bands [39], [40], respectively, and $n = p = 1.5 \times 10^{18}$ cm$^{-3}$ in the active region above lasing threshold [39], $F_c - E_c$ and $F_v - E_v$ are obtained by using the Fermi-Dirac integral [41]. ($E_c$ and $E_v$ are conduction- and valence-band edges, respectively.) By using $E_c - E_v = 0.95$ eV for the quaternary energy gap, the calculated $V_Q$ is 0.98 V.

The voltage distribution may now be used to estimate the current $I_H$ due to the forward-biased InP homojunctions, provided that $I_H \ll I_Q$ and the effects of $I_H$ on the voltage distribution are therefore negligible. The homojunctions are approximated as ideal diodes [42], and $I_H$ is assumed to be dominated by the electron injection into the p-InP cap region, since the n-InP buffer layer is generally more heavily doped and electrons have considerably higher diffusivity than holes. Therefore [42],

$$I_H \simeq q\, \frac{A_H D_n}{L_n}\, \frac{n_i^2}{p}\, \exp \frac{qV_H}{kT} \tag{4}$$

where $A_H$ is the effective homojunction area, $D_n$ and $L_n$ are electron diffusivity and effective diffusion length, respectively, $n_i$ is the intrinsic carrier concentration, $k$ is the Boltzmann constant, and $V_H = V(W + b, o)$ with $b$ being the transported region width (Fig. 18). The effective homojunction area is defined as $A_H = 2L\Delta b$, with the effective width $\Delta b = \int_W^{W+b} \exp [qV(u, o)/kT]\, du / \exp (qV_H/kT)$, which can be estimated to be approximately the distance in which $V(u, o)$ reduces by $kT/q$ or (as done here) evaluated precisely by numerical integration. In the following calculations, values of $D_n = 78$ cm$^2$/s and $n_i^2 = 1.6 \times 10^{14}$ cm$^{-6}$ are computed from published carrier-transport and band-structure parameters [40], [43], respectively, and a constant $L_n = 1$ $\mu$m is assumed.

It is worth mentioning that the homojunction voltage $V_H$ plays a dominant role in the calculation of $I_H$ from (4). Nevertheless, uncertainties have been introduced due to several simplifying assumptions which have been made. First, a constant effective diffusion length $L_n$ has been used without actually solving the two-dimensional diffusion problems and by neglecting its dependence on the doping concentration. Second, the electron drift current has not been included. For small $I_Q$, the electron drift current is relatively small compared to the electron diffusion current but its importance grows with $I_Q$, since the electric field intensity is proportional to $I_Q$. ($\vec{\mathcal{E}}(u, v) = \vec{\nabla} V(u, v)$). To check the importance of the electron drift current, the electric field intensity $\mathcal{E}(W + b, o)$ has been evaluated after each $I_H$ calculation. When $\mathcal{E}(W + b, o)$ is greater than $kT/qL_n$ (259 V/cm for $L_n = 1$ $\mu$m), electron drift current cannot be neglected and (4) underestimates $I_H$.

Table I shows calculated $I_H$ and related physical parameters as a function of $I_Q$ on a given device. Note that $I_H$ is initially very small but increases exponentially. When $I_H \simeq I_Q$, the voltage along the InP homojunctions calculated for $I_Q$ alone may remain a fair approximation, because the additional electric field for the hole-drift-current component of $I_H$ is small up to approximately one electron-diffusion-length away from the homojunctions and is therefore not expected to significantly affect the homojunction voltage. To avoid additonal uncertainties, however, the following calculations have been restricted to $I_H < 0.1\, I_Q$, except for those in Fig. 19.

The effect of the calculated homojunction current on an otherwise linear $L$-$I$ characteristic is demonstrated in Fig. 19, which is obtained by adding $I_H$ to $I_Q$ for each power output (as illustrated in the insert of Fig. 20). It is seen that, for a given device geometry, the $L$-$I$ linearity improves significantly with increasing $p$. To facilitate comparison with experiment, (4) and (3) can be combined and rearranged into (see Appendix B)

$$I_H \simeq 1 \text{ mA} \cdot \exp [(I_Q - I_1)/I_2] \tag{5}$$

where $I_1$ and $I_2$ are parameters characteristic of the device and are nearly independent of $I_Q$ (cf. Table I). The functional form of (5) is in good agreement with experiment. This is

TABLE I
CALCULATED $I_H$ AND RELATED PARAMETERS AS A FUNCTION OF $I_Q$ FOR $p = 4 \times 10^{17}$ cm$^{-3}$, $a = 5.0$ $\mu$m, $W = 1.0$ $\mu$m, AND $b = 3.0$ $\mu$m

| $I_Q$ (mA) | $V_H$ (volt) | $\Delta b$ ($\mu$m) | $n_p(0)$* (cm$^{-3}$) | $I_H$ (mA) | $I_1$ (mA) | $I_2$ (mA) | $\mathcal{E}_{(W+b,o)}$ (volt/cm) |
|---|---|---|---|---|---|---|---|
| 10 | 1.02 | 2.34 | $4.16\times10^{13}$ | 0.073 | 33.2 | 8.88 | 5.6 |
| 20 | 1.05 | 2.02 | $1.55\times10^{14}$ | 0.235 | 32.4 | 8.52 | 11.1 |
| 30 | 1.08 | 1.74 | $5.97\times10^{14}$ | 0.778 | 32.1 | 8.30 | 16.7 |
| 40 | 1.12 | 1.59 | $2.22\times10^{15}$ | 2.64 | 32.1 | 8.15 | 22.2 |
| 50 | 1.15 | 1.42 | $8.57\times10^{15}$ | 9.11 | 32.2 | 8.05 | 27.9 |
| 60 | 1.19 | 1.33 | $3.19\times10^{16}$ | 31.8 | 32.4 | 7.98 | 33.4 |
| 70 | 1.22 | 1.22 | $1.23\times10^{17}$ | 112.1 | 32.6 | 7.93 | 39.0 |

*$n_p(0) = \frac{n_1^2}{p} \exp \frac{qV_H}{kT}$

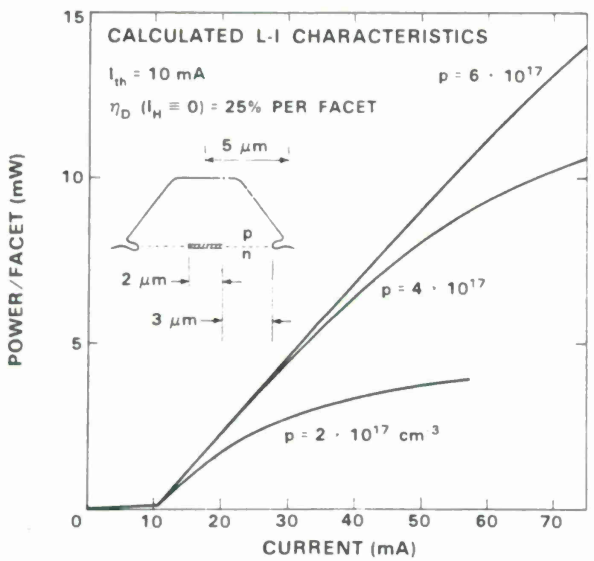


Fig. 19. Sublinear $L$-$I$ characteristics resulting from adding the homojunction current to a linear one. The calculation of the homojunction current was carried out for the device geometry shown in the insert and for three different p-doping concentrations. Note that the numerical value of the curve of $p = 4 \times 10^{17}$ cm$^{-3}$ are listed in Table I.

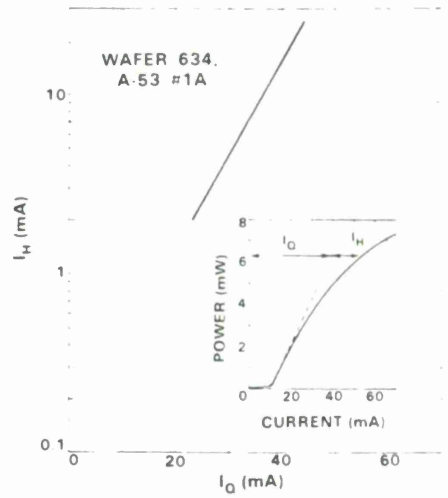


Fig. 20. The relationship between $I_H$ and $I_Q$ which were obtained from an experimental $L$-$I$ characteristic. The insert shows the technique of extracting $I_H$ and $I_Q$ by extrapolating the linear region of the $L$-$I$ characteristic.

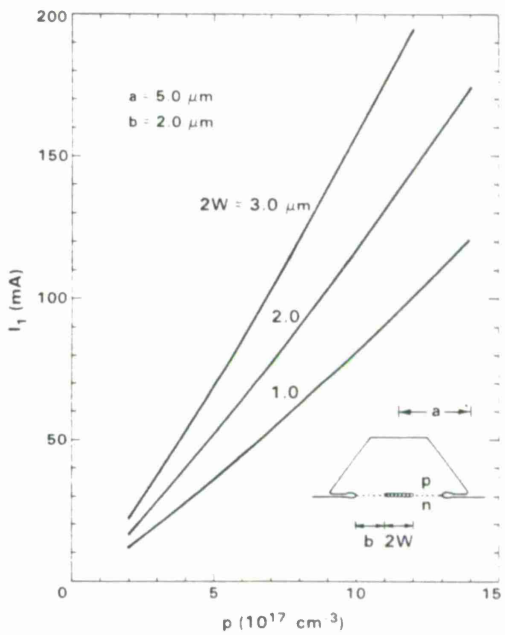


Fig. 21. Calculated $I_1$ as a function of the cap p-doping.

illustrated in Fig. 20 which shows the relationship between $I_H$ and $I_Q$ obtained from an experimental $L$-$I$ characteristic. Note that $I_1$ and $I_2$ provide a convenient characterization of the $L$-$I$ curve. In particular, $I_1$ represents the current limit within which the device should be operated in order that the homojunction current remains small ($I_H < 1$ mA). In the following three paragraphs, calculated $I_1$ for various p-concentrations and device geometries will be presented.

Fig. 21 shows calculated $I_1$ as a function of $p$ for $a = 5.0$ $\mu$m, $b = 2.0$ $\mu$m, and three values of $W$, where $a$, $W$, and $b$ were previously defined but are shown in the insert for convenience. The experimental values of $I_1$ for $p \leqslant 3 \times 10^{17}$ cm$^{-3}$ were 15-26 mA, in general agreement with Fig. 21. A more accurate comparison, however, is not available at present because of the uncertainties in both theory and experiment.

Fig. 22 shows calculated $I_1$ as a function of $b$ for $p = 2$ and $10 \times 10^{17}$ cm$^{-3}$ and three values of $W$. Note that a decrease in $b$ results in relatively small improvement in $I_1$ unless very small $b$ is used. This can be qualitatively explained by noting that the voltage along the homojunctions increases rapidly from the edges of the active region and quickly saturates (see Fig. 18). Therefore, a reduction of $b$ only results in a modest decrease of $V_H$ until $b$ is very small. Furthermore, it should be pointed out that the electric field intensities higher than 259 V/cm are obtained for $b < 1.5$ $\mu$m and, therefore, drift current is not negligible. Smaller values of $I_1$ would be expected if the electron drift current were included in the calculation. Experimentally, $I_1$ as high as 29.5 mA was obtained for $b$ =

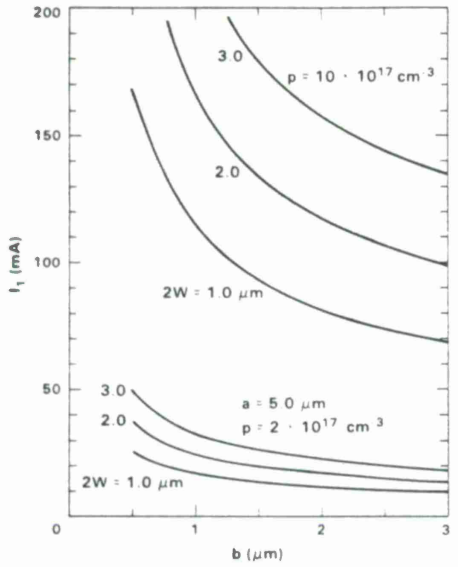


Fig. 22. Calculated $I_1$ as a function of the transported region width $b$.

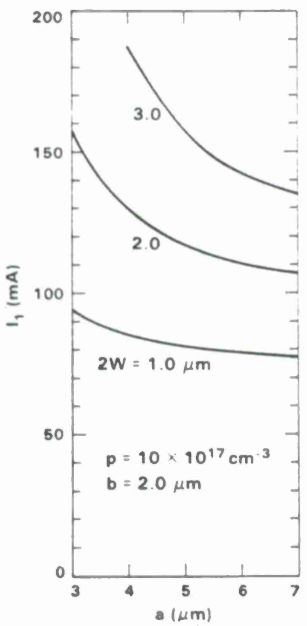


Fig. 23. Calculated $I_1$ as a function of the mesa-base half width $a$.

0.4 μm (Wafer 551 with $2W \simeq 1.1$-1.9 μm as measured on a cleaved bar and $p \leqslant 3 \times 10^{17}$ cm$^{-3}$) but the sublinearity of light output was clearly seen for $I > 30$ mA.

Fig. 23 shows increasing $I_1$ with decreasing mesa width. This can be qualitatively explained by noting that a narrower mesa allows a smaller fraction of a given $I_Q$ to flow laterally and therefore results in less voltage rise for the homojunctions. This is consistent with the fact that $I_1$ increases with $W$ as seen in Figs. 21-23. (cf. Fig. 18.)

The present calculations have been carried out for $\alpha = 0.927$ rad, because this mesa angle was used in recent wafers on which most *L-I* studies were performed. The same calculation technique can be applied to other mesa angles, such as $\alpha = 0.70$ rad for HCl-etched mesas (with stripes parallel to the (011) planes, Fig. 5) and $\alpha \simeq 2.2$ rad for the mesa geometry used by Chen *et al.* [19]. In the case of more conventional BH lasers, the current due to the forward-biased homojunctions can be significantly reduced by proper alignment of the p-n-p-n current-blocking layers, but there are current leakages due to the turn-on [8], [12] or imperfections [14], [44] of the p-n-p-n structure. Circuit models [8], [12], [44] have been developed to diagnose these problems but are evidently more complicated than the present analysis of the mass-transported BH lasers.

## V. Conclusions

Low-threshold, high-efficiency, high device yield and smooth far-field patterns have been obtained for mass-transported GaInAsP/InP BH lasers. Linear light-current characteristics and well-behaved threshold-temperature dependence have been obtained by using sufficient p-doping. The conformal mapping technique allows for rather accurate calculation of the voltage distribution in the laser mesa. The theory is valuable for designing lasers for operation without current leakage through the InP homojunctions.

## Appendix A
## Analytic Expressions for the Transformation on the Real Axes

In calculating the voltage along the InP p-n homojunctions, only the integration along the real axis, from $x = 0$ to $x = a'$, needs to be considered for (2). Let

$$\zeta = \int_0^{\xi} (1 - \xi'^2)^{\alpha/\pi - 1}\, d\xi'. \tag{A1}$$

It can be readily verified that (2) and the requirements that $(x = 1) \rightarrow (u = W)$ and $(x = a') \rightarrow (u = a)$ are satisfied by (A1) if

$$x = a'\xi \tag{A2}$$

$$u = \frac{a}{2.305}\,\zeta \tag{A3}$$

$$a' = \frac{1}{\xi(\zeta = 2.305\ W/a)} \tag{A4}$$

and by noting that $2.305 = \int_0^1 (1 - \xi'^2)^{\alpha/\pi - 1}\, d\xi'$, with $\alpha = 0.927$.

The integral of (A1) has been evaluated numerically and is shown in Fig. 24. To avoid the tedious task of numerical integration, approximate analytic expressions have been obtained by expanding the integrand into power series at $\xi = 0$ and at $\xi = 1$ and by integrating the series term by term:

$$\zeta \simeq \begin{cases} (1 + 0.2349\,\xi^2 + 0.1202\,\xi^4)\,\xi \\ \qquad\qquad \text{for } 0 \leqslant \xi \leqslant 0.5 \qquad \text{(A5a)} \\ 2.305 - 2.0785\,(1 - \xi)^{0.2952}\,[1 + 0.0803\,(1 - \xi) \\ \qquad + 0.0193\,(1 - \xi)^2] \quad \text{for } 0.5 < \xi \leqslant 1.0. \qquad \text{(A5b)} \end{cases}$$

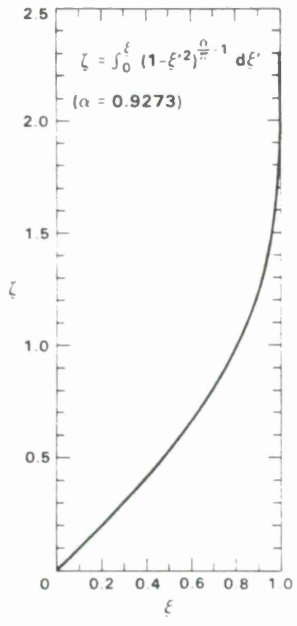


Fig. 24. Plot of the integral $\zeta = \int_0^{\xi} (1 - \xi'^2)^{\alpha/\pi - 1}\, d\xi'$, with $\alpha = 0.9273$. Note that $\zeta = 2.305$ when $\xi = 1$.

These series can be reversed to yield

$$\xi \simeq \begin{cases} (1 - 0.2349\,\zeta^2 + 0.04533\,\zeta^4)\,\zeta \\ \quad \text{for } 0 \leqslant \zeta \leqslant 0.534 \end{cases} \tag{A6a}$$

$$\begin{cases} 1 - R + 0.272\,R^2 - 0.0565\,R^3 \\ \quad \text{for } 0.534 < \zeta \leqslant 2.305 \end{cases} \tag{A6b}$$

where $R = [(2.305 - \zeta)/2.0785]^{1/0.2952}$. Equations (A5) and (A6) yield approximations to within 0.2 percent of the exact values.

Expressions for $x(u)$ (i.e., the transformation on the real axes) are then obtained directly from (A6) by using the change of variables defined in (A2)-(A4). Combined with $\Phi = \ln(x + \sqrt{x^2 - 1})$ for $x > 1$ on the real axis [cf. (1)], expressions for $\Phi(u, o)$ are obtained. Note that $\Phi(u, o)$ is all that is needed [instead of the entire $\Phi(u, v)$] in (4) calculation of $I_H$.

## Appendix B
## Expressions for $I_1$ and $I_2$

Define

$$I_o = \frac{A_H D_n}{L_n} \frac{n_i^2}{p} \exp \frac{qV_Q}{kT}. \tag{B1}$$

Then, by using (3) for $V_H$, (4) becomes

$$I_H \simeq I_o \exp\left(\frac{q}{kT} \frac{\rho \Phi_H}{\pi L} I_Q\right) \tag{B2}$$

where $\Phi_H = \Phi(W + b, O)$. Equation (B2) can be transformed into (5) by letting

$$I_2 = \frac{kT}{q} \Big/ \frac{\rho \Phi_H}{\pi L} \tag{B3}$$

and

$$I_1 = I_2 \ln(1\ \text{mA}/I_o). \tag{B4}$$

Note that $I_2$ as defined in (B3) is independent of $I_Q$, but $I_1$ is not, because $I_o$ has an $I_Q$-dependence through $A_H$. Since $I_1$ and $I_2$ are not both constant, the assignment of $I_1$ and $I_2$ for (5) is actually somewhat arbitrary.

*Note Added in Proof:* A recent recalibration of our Ge photodiode (at 1.322 $\mu$m wavelength by using an NBS traceable Laser Precision Rs-3960 electrically calibrated pyroelectric radiometer) shows that the output power and differential quantum efficiency values reported in this paper should be multiplied by 1.2-1.26. Also, a room-temperature CW light output of 30 mW per facet (after the detector recalibration) has been achieved at a current of 158 mA (which is over ten times the threshold) on a recently packaged device from Wafer 615.

## Acknowledgment

The authors wish to thank D. E. Mull for LPE growth and characterization of the starting wafers, L. J. Missaggia for device processing, W. F. McBride for device packaging, S. H. Groves, J. J. Hsieh, and C. E. Hurwitz for valuabie discussions, G. W. Iseler for growing the InP ingots, B. DiGiorgio, S. Duda, and A. Napoleone for substrate slicing and polishing, P. M. Nitishin for part of the SEM work, and F. J. Leonberger and R. C. Williamson for encouragement.

## References

[1] J. J. Hsieh and C. C. Shen, "Room-temperature CW operation of buried-stripe double-heterostructure GaInAsP/InP diode lasers," *Appl. Phys. Lett.*, vol. 30, pp. 429-431, Apr. 15, 1977.

[2] H. Kano and K. Sugiyama, "Operation characteristics of buried-stripe GaInAsP/InP DH lasers made by melt-back method," *J. Appl. Phys.*, vol. 50, pp. 7934-7938, Dec. 1979.

[3] M. Hirao, A. Doi, S. Tsuji, M. Nakamura, and K. Aiki, "Fabrication and characterization of narrow stripe InGaAsP/InP buried heterostructure lasers," *J. Appl. Phys.*, vol. 51, pp. 4539-4540, Aug. 1980.

[4] R. J. Nelson, R. B. Wilson, P. D. Wright, P. A. Barnes, and N. K. Dutta, "CW electrooptical properties of InGaAsP ($\lambda$ = 1.3 $\mu$m) buried-heterostructure lasers," *IEEE J. Quantum Electron.*, vol. QE-17, pp. 202-207, Feb. 1981.

[5] S. Arai, M. Asada, T. Tanbun-Ek, Y. Suematsu, Y. Itaya, and K. Kishino, "1.6 $\mu$m wavelength GaInAsP/InP BH lasers," *IEEE J. Quantum Electron.*, vol. QE-17, pp. 640-645, May 1981.

[6] P. C. Chen, K. L. Yu, S. Margalit, and A. Yariv, "Embedded epitaxial growth of low-threshold GaInAsP/InP injection lasers," *Appl. Phys. Lett.*, vol. 38, pp. 301-303, Mar. 1, 1981.

[7] W. Ng, C. S. Hong, H. Manasevit, and P. D. Dapkus, "Low-threshold 1.3-$\mu$m GaInAsP/InP buried heterostructure lasers by liquid phase epitaxy and metalorganic chemical vapor deposition," *Appl. Phys. Lett.*, vol. 39, pp. 188-189, Aug. 1, 1981.

[8] Y. Nakano, K. Takahei, Y. Noguchi, Y. Suzuki, and H. Nagai, "Output power saturation of BH laser under high current injection," *Electron. Lett.*, vol. 18, pp. 501-502, June 10, 1982.

[9] K. L. Yu, U. Koren, T. R. Chen, and A. Yariv, "A groove GaInAsP laser on semi-insulating InP using a laterally diffused junction," *IEEE J. Quantum Electron.*, vol. QE-18, pp. 817-819, May 1982.

[10] H. Ishikawa, H. Imai, T. Tanahashi, K. Hori, and K. Takahei, "V-grooved substrate buried heterostructure InGaAsP/InP laser emitting at 1.3 $\mu$m wavelength," *IEEE J. Quantum Electron.*, vol. QE-18, pp. 1704-1711, Oct. 1982.

[11] D. L. Murrell, R. H. Walling, R. E. Hobbs, and W. J. Devlin, "Formation of a long-wavelength buried-crescent laser structure on channeled substrates," *IEE Proc.*, vol. 129, pt. I, pp. 209-212, Dec. 1982.

[12] H. Namizaki, R. Hirano, H. Higuchi, E. Oomura, Y. Sakakibara, and W. Susaki, "Shunt current and excess temperature sensitivity of $I_{th}$ and $\eta_{ex}$ in 1.3 $\mu$m InGaAsP DH lasers," *Electron. Lett.*, vol. 18, pp. 703-705, Aug. 5, 1982.

[13] R. A. Logan, J. P. van der Ziel, H. Temkin and C. H. Henry, "InGaAsP/InP (1.3 $\mu$m) buried-crescent lasers with separate optical confinement," *Electron. Lett.*, vol. 18, pp. 895-896, Sept. 30, 1982.

[14] R. Plastow, M. Harding, I. Griffith, A. C. Carter, and R. C. Goodfellow, "Low-threshold current CW operation of multiple infil buried heterostructure 1.3 μm GaInAsP lasers," *Electron. Lett.*, vol. 18, pp. 262–263, Mar. 18, 1982.

[15] I. Mito, M. Kitamura, K. Kobayashi, S. Murata, M. Seki, Y. Odagiri, H. Nishimoto, M. Yamaguchi, and K. Kobayashi, "InGaAsP double-channel-planar-buried-heterostructure laser diode (DC-PBH LD) with effective current confinement," *J. Lightwave Technol.*, vol. LT-1, pp. 195–202, Mar. 1983.

[16] M. Oron and N. Tamari, "High power single mode InGaAsP lasers fabricated by single step liquid phase epitaxy," *Appl. Phys. Lett.*, vol. 42, pp. 139–141, Jan. 15, 1983.

[17] Z. L. Liau and J. N. Walpole, "A novel technique for GaInAsP/InP buried heterostructure laser fabrication," *Appl. Phys. Lett.*, vol. 40, pp. 568–570, Apr. 1, 1982; *IEEE Trans. Electron Dev.*, vol. ED-29, p. 1675, Oct. 1982.

[18] T. R. Chen, L. C. Chiu, K. L. Yu, U. Koren, A. Hasson, S. Margalit, and A. Yariv, "Low threshold InGaAsP terrace mass transport laser on semi-insulating substrate," *Appl. Phys. Lett.*, vol. 41, pp. 1115–1117, Dec. 15, 1982.

[19] P. C. Chen, H. D. Law, E. A. Rezek, and J. Weller, "Monolithic integration of laser-FET on InP," *Tech. Dig., IOOC'83* (IECE of Japan, Tokyo), pp. 190–191, June 1983.

[20] Z. L. Liau, J. N. Walpole, and D. Z. Tsang, "New developments in mass-transported GaInAsP/InP buried-heterostructure lasers," *Tech. Dig., IOOC'83* (IECE of Japan, Tokyo), pp. 152–153, June 1983.

[21] M. Ayabe, H. Nagasawa, and K. Kaneko, "Vapor-phase transport of GaAs on a *V*-shape grooved GaAs substrate," *J. Cryst. Growth*, vol. 58, pp. 180–184, June 1982.

[22] T. R. Chen, L. C. Chiu, A. Hasson, K. L. Yu, U. Koren, S. Margalit, and A. Yariv, "Study and application of the mass transport phenomenon on InP," *J. Appl. Phys.*, vol. 54, pp. 2407–2412, May 1983.

[23] A. W. Nelson, L. D. Westbrook, and J. S. Evans, "Deformation-free overgrowth of InGaAsP DFB corrugations," *Electron. Lett.*, vol. 19, pp. 34–36, Jan. 20, 1983.

[24] J. Kinoshita, H. Okuda, and Y. Uematsu, "Preserving InP surface corrugations for 1.3 μm GaInAsP/InP DFB lasers from thermal deformation during LPE process," *Electron. Lett.*, vol. 19, pp. 215–216, Mar. 17, 1983.

[25] H. Nagai, Y. Noguchi, T. Matsuoka, and Y. Suzuki, "Prevention of surface corrugation thermal deformation for InGaAsP/InP DFB lasers," *Japan. J. Appl. Phys.*, vol. 22, pp. L291–L293, May 1983.

[26] A. Hasson, L. C. Chiu, T. R. Chen, U. Koren, Z. Rav-Noy, K. L. Yu, S. Margalit, and A. Yariv, "Selective low-temperature mass transport in InGaAsP/InP lasers," *Appl. Phys. Lett.*, vol. 43, pp. 403–405, Sept. 1, 1983.

[27] M. Feng, T. H. Windhorn, M. M. Tashima, and G. E. Stillman, "Liquid-phase epitaxial growth of lattice-matched InGaAsP on (100)-InP for the 1.15–1.31 μm spectral region," *Appl. Phys. Lett.*, vol. 32, pp. 758–761, June 1, 1978.

[28] The wafer numbers are assigned in the chronological order of the wafer growths and are cited in this paper for cross-reference purposes.

[29] U. Koren, T. R. Chen, C. Harder, A. Hasson, K. L. Yu, L. C. Chiu, S. Margalit, and A. Yariv, "InGaAsP/InP undercut mesa laser with planar polyimide passivation," *Appl. Phys. Lett.*, vol. 42, pp. 403–405, Mar. 1, 1983.

[30] L. A. Coldren, K. Furuya, and B. I. Miller, "On the formation of planar-etched facets in GaInAsP/InP double heterostructure," *J. Electrochem. Soc.*, vol. 130, pp. 1918–1926, Sept. 1983.

[31] C. H. Henry, R. A. Logan, and F. R. Merritt, "Single mode operation of buried heterostructure lasers by loss stabilization," *IEEE J. Quantum Electron.*, vol. QE-17, pp. 2196–2204, Nov. 1981.

[32] Y. Itaya, Y. Suematsu, S. Katayama, K. Kishino, and S. Arai, "Low threshold current density (100) GaInAsP/InP double-heterostructure lasers for wavelength 1.3 μm," *Japan. J. Appl. Phys.*, vol. 18, pp. 1795–1805, Sept. 1979.

[33] W. Ng and Y. Z. Liu, "Effect of p-doping on carrier lifetime and threshold current density of 1.3 μm GaInAsP/InP lasers by liquid-phase epitaxy," *Electron. Lett.*, vol. 16, pp. 693–695, Aug. 28, 1980.

[34] P. J. Anthony and N. E. Schumaker, "Temperature dependence of the lasing threshold current of double heterostructure injection lasers due to drift current loss," *J. Appl. Phys.*, vol. 15, pp. 5038–5040, Sept. 1980.

[35] C. B. Su, J. Schlafer, J. Manning, and R. Olshansky, "Measurement of radiative recombination coefficient and carrier leakage in 1.3 μm InGaAsP lasers with lightly doped active layers," *Electron. Lett.*, vol. 18, pp. 1108–1110, Dec. 9, 1982.

[36] T. R. Chen, B. Chang, L. C. Chiu, K. L. Yu, S. Margalit, and A. Yariv, "Carrier leakage and temperature dependence of InGaAsP lasers," *Appl. Phys. Lett.*, vol. 43, pp. 217–218, Aug. 1, 1983.

[37] W. R. Smythe, *Static and Dynamic Electricity*, 3rd ed. New York: McGraw-Hill, 1968, ch. 4.

[38] F. B. Hildebrand, *Advanced Calculus for Applications.* New York: Prentice-Hall, 1962, ch. 10.

[39] N. K. Dutta, "Calculated absorption, emission and gain in $In_{0.72}Ga_{0.28}As_{0.6}P_{0.4}$," *J. Appl. Phys.*, vol. 51, pp. 6095–6100, Dec. 1980.

[40] T. P. Pearsall, Ed., *GaInAsP Alloy Semiconductors.* New York: Wiley, 1982, ch. 12.

[41] H. C. Casey, Jr. and M. B. Panish, *Heterostructure Lasers, Part A.* New York: Academic, 1978, ch. 4.

[42] A. S. Grove, *Physics and Technology of Semiconductor Devices.* New York: Wiley, 1967, ch. 6.

[43] H. C. Casey, Jr. and M. B. Panish, *Heterostructure Lasers, Part B.* New York: Academic, 1978, ch. 5.

[44] P. D. Wright, W. B. Joyce, and D. C. Craft, "Electrical derivative characteristics of InGaAsP buried heterostructure lasers," *J. Appl. Phys.*, vol. 53, pp. 1364–1372, Mar. 1982.

**Z. L. Liau** was born in Taipei, Taiwan, in 1950. He received the B.S. degree in physics from the National Taiwan University, Taipei, Taiwan, in 1972, and the Ph.D. degree in applied physics from the California Institute of Technology, Pasadena, in 1978.

Since December 1978 he has been a staff member in the Applied Physics Group, Lincoln Laboratory, Massachusetts Institute of Technology, Lexington, where his work has been on GaInAsP/InP lasers, including liquid-phase epitaxy, buried heterostructure, and monolithic integration with passive waveguides.

**James N. Walpole** received the B.S.E.E. degree in 1961 from Duke University, Durham, NC, and the M.S. and Ph.D. degrees from the Department of Electrical Engineering, Massachusetts Institute of Technology, Cambridge, in 1962 and 1966, respectively. His major studies were in the areas of solid-state physics and semiconductor devices.

He was appointed Assistant Professor of Electrical Engineering at the Massachusetts Institute of Technology in 1966 and Associate Professor in 1971. Since 1972 he has been a Staff Member in the Applied Physics Group, Lincoln Laboratory, Massachusetts Institute of Technology, Lexington, where he is currently involved with development of GaInAsP heterostructure lasers. His previous research interests have centered on the physics of the lead–tin chalcogenide semiconductors including studies of magnetoplasma wave propagation, diffusion, hot-electron conduction, metal-semiconductor contacts, and various aspects of injection lasers in these materials.

**Dean Z. Tsang** (S'73–M'80–S'81–M'81) was born in Detroit, MI, on August 13, 1952. He received the S.B. degree from the Massachusetts Institute of Technology, Cambridge, the M.S. degree from the University of Illinois, Urbana-Champaign, and the Sc.D. degree from the Massachusetts Institute of Technology, all in electrical engineering.

In 1975 he came to the M.I.T. Lincoln Laboratory, Lexington, MA, as a graduate student where he was involved with lead salt diode lasers, integrated optics, and *Q*-switched diode lasers. He is currently working as a Staff Member on GaInAsP diode lasers.

# APPENDIX B

# *Q* switching of low-threshold buried-heterostructure diode lasers at 10 GHz

D. Z. Tsang, J. N. Walpole, Z. L. Liau, S. H. Groves, and V. Diadiuk
*Lincoln Laboratory, Massachusetts Institute of Technology, Lexington, Massachusetts 02173-0073*

(Received 9 April 1984; accepted for publication 14 May 1984)

Buried-heterostructure actively *Q*-switched diode lasers have been made with threshold currents as low as 14 mA. The lasers operate continuously at room temperature. Modulation has been observed at rates up to 10.5 GHz. Evidence of several modes of *Q* switching has been obtained.

*Q*-switched diode lasers are of interest for high-bandwidth optical fiber communication systems.[1–5] Laser pulses at modulation rates of several tens of gigahertz should be possible.[5] Previously reported actively *Q*-switched semiconductor lasers with an integrated electroabsorption modulator have been operated on a pulsed basis with thresholds of 240 mA.[3,5] A two-section buried-heterostructure laser with a proton-isolated modulator was also reported.[6] These devices had a threshold of about 40 mA and were *Q* switched at 3 GHz. Here, we report buried-heterostructure *Q*-switched lasers[7] with thresholds as low as 14 mA at an emission wavelength of 1.3 $\mu$m. The capacitance of the intracavity electroabsorption modulator can be as low as 0.1 pF under reverse bias. Since the capacitance is small and only a few volts of reverse bias are required, the laser can be easily modulated when integrated with low-power high-speed transistors without the high current drive required for direct-current modulation. The devices have been continuously operated with full on/off modulation at rates of at least 10 GHz.

The design, fabrication, and operation of the laser are similar to the zinc-diffused stripe *Q*-switched lasers reported earlier[3,5] except for modifications made to incorporate the buried heterostructure. The laser is fabricated from a double-heterostructure wafer consisting of a $2\times10^{18}$ cm$^{-3}$ Sn-doped buffer layer, a $1\times10^{16}$ cm$^{-3}$ *n*-type $Ga_{0.26}In_{0.74}As_{0.60}P_{0.40}$ active layer, and a $1\times10^{16}$ cm$^{-3}$ *n*-type InP cap layer. Both selective chemical etching to define an active region about 2 $\mu$m wide and a mass transport process[8] to bury the active region are used to form the buried heterostructure. Zinc is selectively diffused to form an amplifier section and beryllium is selectively implanted to form a modulator section as shown in Fig. 1. Au-Zn contacts are applied to the *p*-type regions and a Au-Sn contact is applied to the *n*-type substrate. Mirrors are formed by cleaving. The amplifier is forward biased to produce optical gain while the modulator is reverse biased to produce optical loss. The modulator design is based on the use of electroabsorption (Franz–Keldysh effect). For optical energies slightly less

 0003-6951/84/150204-03$01.00  

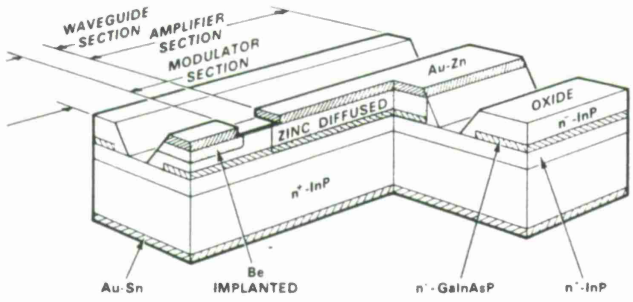


FIG. 1. Perspective cutaway view of the $Q$-switched laser. The buried-heterostructure active region extends through all three sections of the device.

than the band gap of the GaInAsP layer, the optical absorption can be controlled by the electric field produced in the modulator *pn* junction. The bulk absorption in the GaInAsP layer can be increased from a very small value to over 1000 $cm^{-1}$ as the electric field is varied from zero to $>3.6\times10^5$ V/cm for photon energies as much as 60 meV below the energy gap.[9] The amplifier and modulator are optically coupled but electrically isolated by the waveguide section. The cross section of the buried heterostructure is constant throughout the device. The active region is about 0.2 $\mu$m thick and 2 $\mu$m wide. The position of the beryllium-implanted junction is deliberately offset from the quaternary layer as shown in Fig. 1 to prevent electroabsorption at zero bias.[3] Typically the length of the amplifier is 150–250 $\mu$m while the length of the modulator is 25–75 $\mu$m. The waveguide section is 25 $\mu$m long.

The laser is mounted in a package between two microstriplines which bring the electrical drive signals to the two sections. In order to facilitate bonding, the device is mounted with the substrate side soldered to the heatsink.

The lasers have thresholds as low as 14 mA with the modulator open circuited. The low threshold of the lasers permits continuous operation at room temperature. In order to characterize the modulator loss, the threshold of the laser can be measured as a function of the modulator reverse bias. At a 13-V reverse bias the pulsed threshold for one device (Fig. 2) increases by a factor of about 4.5 compared to the threshold with the modulator open circuited, indicating a substantial variation in intracavity loss.

The devices were modulated by application of both a dc

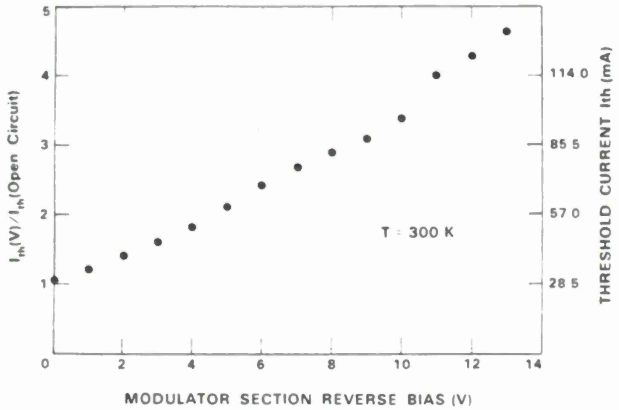


FIG. 2. Pulsed threshold, normalized to the threshold of the laser with the modulator open, as a function of modulator reverse bias.

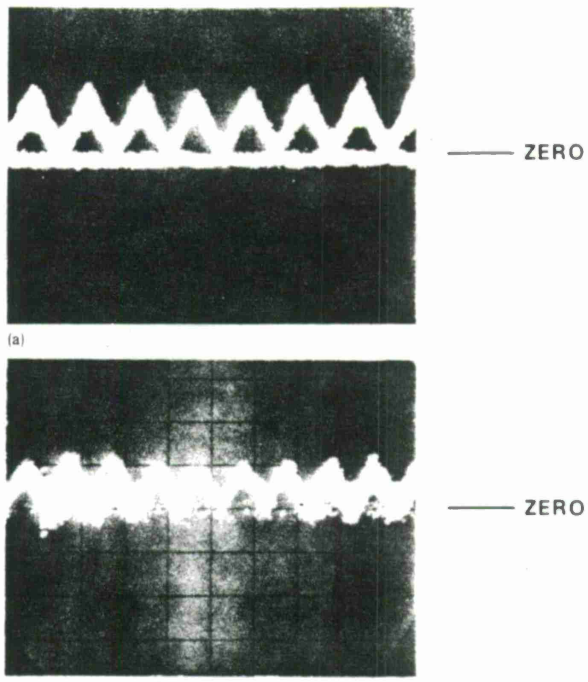


FIG. 3. (a) Continuous $Q$ switching at 8 GHz; (b) $Q$ switching at 10.2 GHz. Both figures have an extra trace to show the reference level with the light blocked. The intensity of the reference was reduced in (b).

voltage and a microwave signal to the modulator.[5] Typically 70–200 mW of microwave power and a few volts of dc reverse bias were sufficient to drive the unmatched modulator. The devices were modulated at rates between 2 and 10.5 GHz. The optical pulses out of the laser were collected and focused on a back-illuminated 25-$\mu$m-diam GaInAs/InP *pin* photodiode with less than 70-ps full width at half-maximum response time.[10] The detector output was displayed on a sampling oscilloscope with a 20-ps rise time. Continuous $Q$-switched operation at a rate of 8 GHz with full on/off modulation is illustrated in Fig. 3(a). The laser amplifier was driven at 2.1 times the threshold of the device with the modulator open. The modulator was dc biased with 1.3-V reverse bias. 100 mW of microwave power was applied to the system. The actual modulator drive power was somewhat less due to insertion losses in the bias tee, cables, and connectors. Full on/off modulation was seen at 10.2 GHz as shown in Fig. 3(b), although the detected signal is smaller. In addition, modulation up to 10.5 GHz was observed although the signal is smaller still.

Various types of behavior including subharmonic operation and irregular pulsations can be seen when the operating conditions of the laser are varied. The effect of increases in the amplifier current at a fixed modulation frequency of 2 GHz is shown in Fig. 4. When the amplifier current was just sufficient to produce laser oscillation, laser pulses were observed at the modulation frequency as shown in Fig. 4(a). With increasing current, the intensity of the pulses increased, Fig. 4(b), until a transition region in which the laser pulses irregularly was encountered, Fig. 4(c). With still higher current, the laser again operated at the fundamental of the modulation frequency [Fig. 4(d)].

The qualitative behavior of the device can be under-

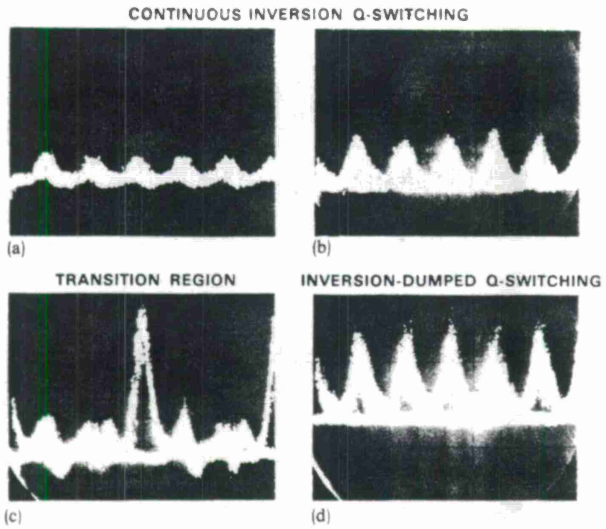


FIG. 4. Effect of increasing the amplifier current (a) 50 mA, (b) 54 mA, (c) 59 mA, and (d) 68 mA at 2 GHz with the modulator drive held constant. The dc threshold of this laser is 30 mA with the modulator open. (b)–(d) have an extra trace which shows the zero reference obtained when the light is blocked.

stood from previous modeling (cf. Fig. 7, Ref. 5). Just above threshold in Fig. 4(a), the electrons do not have sufficient time to recombine radiatively and most of the population remains in the inverted state. The device operates in a continuous-inversion mode of $Q$ switching[5] in which the population inversion remains continuously high. In this mode, each time the modulator loss is lowered, a pulse is emitted without the time delay associated with rebuilding the electron population. In Fig. 4(b) the intensity of the pulses increases with the amplifier current because the gain increases. The modeling also suggests that as the current increases still further, the laser moves into a transition region in which the population intermittently reaches a level sufficient to dump below its low-loss threshold value (the population at threshold when the modulator loss is low) and does not recover to produce pulses at the modulation frequency as in Fig. 4(c). Finally, when the level of pumping increases sufficiently, the population recovers regularly and pulses are produced at the modulation frequency as shown in Fig. 4(d). In this mode of operation the population regularly dumps below threshold. The height of the pulses in Figs. 4(a) and 4(b) compared to Figs. 4(c) and 4(d) is consistent with inversion-dumped $Q$-switched operation since large pulses are expected when the population rapidly drops below its low-loss threshold. The present results provide the first experimental evidence of a continuous-inversion $Q$-switching mechanism.

The results reported here demonstrate $Q$-switched diode lasers with low threshold current. The lasers have been modulated at rates of 10 GHz and should be useful for optical fiber communication systems and other applications requiring such high rates.

The authors would like to thank L. P. Hammond for the fabrication of the laser devices, M. C. Plonko for assistance with the growth of the LPE layers, J. D. Woodhouse and R. Poillucci for the ion implantation, and F. McBride for the packaging. The authors would also like to thank G. W. Iseler for the InP substrate material and W. F. DiNatale for fabrication of the detectors. This work was supported by the Departments of the Air Force, the Navy and the Defense Advanced Research Projects Agency.

[1]T. Tsukada and C. L. Tang, IEEE J. Quantum Electron. **QE-13**, 37 (1977).
[2]M. Yamanishi, K. Ishii, M. Ameda, and T. Kawamura, Jpn. J. Appl. Phys. **17**, Suppl. 359 (1978).
[3]D. Z. Tsang, J. N. Walpole, S. H. Groves, J. H. Hsieh, and J. P. Donnelly, Appl. Phys. Lett. **38**, 120 (1981).
[4]H. Ito, N. Onodera, K. Gen-Ei, and H. Inaba, Electron. Lett. **17**, 15 (1981).
[5]D. Z. Tsang and J. N. Walpole, IEEE J. Quantum Electron. **QE-19**, 145 (1983).
[6]D. Z. Tsang, J. N. Walpole, and Z. L. Liau, IEEE Trans. Electron Devices **ED-30**, 1596 (1983).
[7]D. Z. Tsang, J. N. Walpole, Z. L. Liau, and S. H. Groves, in 4th Int. Conf. Integrated Opt. Optical Fiber Commun. postdeadline Technical Digest, Tokyo, Japan, June 27–30, 1983, paper 29B5-6.
[8]Z. L. Liau and J. N. Walpole, Appl. Phys. Lett. **40**, 568 (1982); IEEE Trans. Electron Devices **ED-29**, 1675 (1982).
[9]R. H. Kingston, Appl. Phys. Lett. **34**, 744 (1979).
[10]V. Diadiuk, S. H. Groves, D. Z. Tsang, and J. N. Walpole, IEEE Trans. Electron Devices **ED-30**, 1608 (1983).

# APPENDIX C

# Low threshold GaInAsP/InP buried-heterostructure lasers with a chemically etched and mass-transported mirror

Z. L. Liau, J. N. Walpole, and D. Z. Tsang
*Lincoln Laboratory, Massachusetts Institute of Technology, Lexington, Massachusetts 02173-0073*

(Received 16 January 1984; accepted for publication 6 March 1984)

The mass-transport technique has been used to improve chemically etched mirrors on GaInAsP/InP double heterostructure wafers. Vertical and flat mirror facets have been obtained. Buried-heterostructure lasers fabricated with one such mirror and the other mirror cleaved show high device yield with threshold currents as low as 6 mA and differential quantum efficiency as high as 33%.

PACS numbers: 42.55.Px, 42.78.Cf, 81.60. – j, 73.40.Lq

There has been considerable interest in heterostructure lasers with etched [1–6] or micro-cleaved[7,8] mirrors, because they are potentially very important for monolithic optoelectronic integration, coupled cavity and short cavity lasers, and batch processing. The chemically etched mirrors reported to date, however, were generally not flat[1–3,9,10] or not perpendicular[1,2] to the active layer and resulted in degraded mode reflectivity. Moreover, the vertical facets which can be produced by wet chemical etching on (100) substrates are generally parallel to $(01\bar{1})$ planes[9–12] and therefore cannot be easily applied to the conventional buried-heterostructure (BH) lasers. [These important laser structures[13,14] are usually fabricated with stripe edges parallel to $(01\bar{1})$ planes in order to achieve desired active region width and high quality layer growth.] As a result, GaInAsP/InP lasers with etched mirrors reported to date[1–5] showed threshold currents considerably higher than those with cleaved mirrors.[13–19]

The recently developed mass-transport technique[15–18] offers new possibilities for solution of the above-mentioned problems. It not only allows high quality BH lasers to be fabricated with stripe edges perpendicular to $(01\bar{1})$ planes[15,18] but also can be used in a new procedure described here to smooth out defects in chemically etched mirrors near the active layer. Such lasers have been realized in the present work and promising initial results of high device yield, low threshold current, and high differential quantum efficiency are reported in this letter.

The present experiment starts with a mass-transported BH laser wafer similar to those previously reported,[15,18] except that a planar region is retained at the end of each laser mesa, as illustrated in Fig. 1(a). The wafer is first treated in an aqueous solution of $K_3Fe(CN)_6$ and KOH and then a $SiO_2$ (or phosphosilicate glass, PSG) layer is pyrolytically deposited. Photolithographic techniques are subsequently used to open up the $SiO_2$ layer in the planar end region, as shown in Fig. 1(a). The longitudinal cross section of the laser mesa at this stage is illustrated in Fig. 2(a). The wafer is then cleaned and steps of selective chemical etching are taken in order to obtain the profile shown in Fig. 2(b). First, a mixture of $H_3PO_4$ and HCl is used to remove the unprotected InP cap layer.[11,12] Second, an aqueous solution of $K_3Fe(CN)_6$ and KOH is used to remove the exposed GaInAsP active layer. These two etching steps are then repeated until the desired profile in Fig. 2(b) is obtained. The wafer is then loaded into a furnace system for mass transport[15] at a temperature of 670–690 °C in order to form a smooth mirror facet as illustrated in Fig. 2(c). The mirror facet is thus formed by chemical etching followed by the mass-transport procedure and will be designated as the "transported mirror" for convenience in the rest of the paper.

A number of experiments have been carried out in order to determine the optimum etching and transport parameters. For example, the surface treatment prior to the $SiO_2$ or PSG deposition has been found to be important in preventing large and irregular undercuts in the subsequent chemical etching. Also, higher transport temperatures have been found to be more effective in smoothing the mirror facet. As a result, essentially vertical and flat mirrors are obtained with good reproducibility. Figures 3(a) and 3(b) show scanning electron microscope (SEM) photographs of the longitudinal cross sections of samples before and after the mass transport. [cf. Figs. 2(b) and 2 (c)]. Note that steps are seen across the active layer in the sample before transport, and a smooth mirror surface is obtained after transport. Near the transported mirror, the GaInAsP active layer terminates 0.1–0.3 $\mu$m short of the all-InP mirror surface. Figure 3(c) shows an SEM perspective view of a laser end region with a transported mirror [cf. Fig. 1(b)]. For comparison, a similar photograph of a cleaved facet is shown in Fig. 3(d). These photographs further demonstrate the flatness and smoothness of the transported mirror.

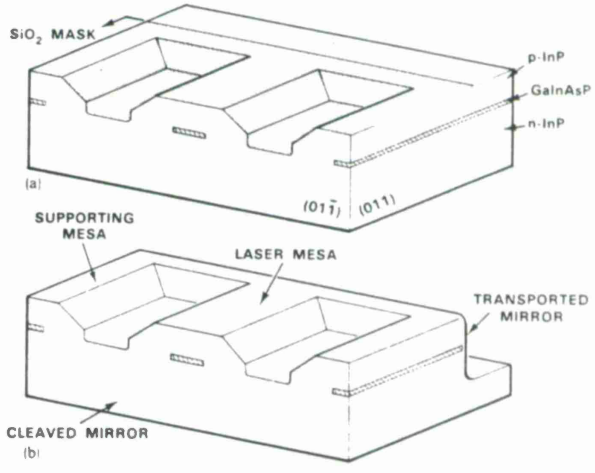


FIG. 1. Schematic pictures of the BH wafer (a) before and (b) after the formation of the transported mirror.

 0003-6951/84/100945-03$01.00  

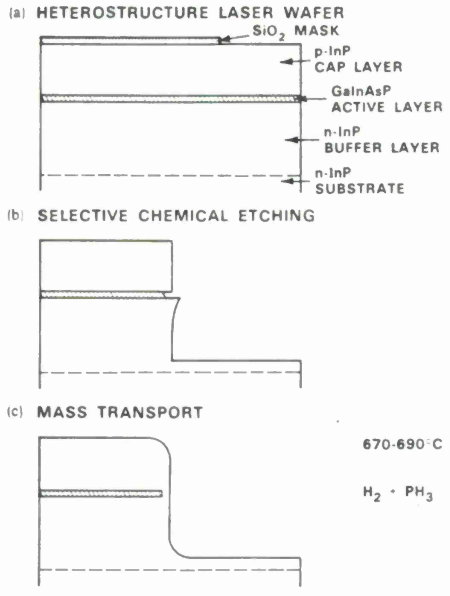


FIG. 2. Procedures for the formation of the transported mirror.

After the formation of the transported mirrors, the wafer is processed into BH lasers by using the metallization (over a PSG insulating layer which has openings on top of the laser mesas) and dicing procedures similar to those described previously.[15] The finished lasers have one transported mirror and one cleaved mirror [cf. Fig. 1(b)]. The lasers are then conveniently characterized by using the emission from the cleaved mirror, because the transported mirror is coated with PSG and Ti/Au layers due to the above-mentioned metallization procedures. In this respect, the arrangement is similar to that of Iga and Miller (cf. Fig. 5 of Ref. 1).

A high yield of low threshold BH lasers has been obtained. For example, 70% of some 50 devices tested for wafer 655 show threshold currents below 30 mA. Approximately half of these good devices have threshold currents between 6 and 10 mA, with laser cavity lengths ranging from 75 to 150 $\mu$m and estimated active region width and thickness of 3 and 0.18 $\mu$m, respectively. Figure 4 shows the cw light-current characteristic and emission spectra of one device. Nearly single longitudinal mode operation is obtained at 50% above threshold, and the differential quantum efficiency is 33% at the same current level. It is worth noting that, although the device is mounted $p$ side up on the copper heatsink, the cw threshold current is the same as the pulsed. Nevertheless, the sublinearity in the light-current characteristic at higher current could partially be due to heating.

It should be noted that the present threshold currents are significantly lower than the $>50$ mA values previously reported for GaInAsP/InP lasers with etched mirrors[1–5] and are comparable to the lowest achieved for the lasers with both mirrors cleaved.[8,13–19] Nevertheless, still lower threshold current, higher differential quantum efficiency and better mode behavior should be expected. Improvements might be obtained by using better mirror coating (the PSG/Ti/Au employed in this work does not have good reflectivity at 1.3-$\mu$m wavelength) and a shorter cavity.[20]

It is worth mentioning that the quaternary active region near the transported mirror is totally buried in InP, as evident in Figs. 3(b) and 3(c). The transported mirror is therefore "passivated" and has the potential for better reliability and for transmitting higher power densities.

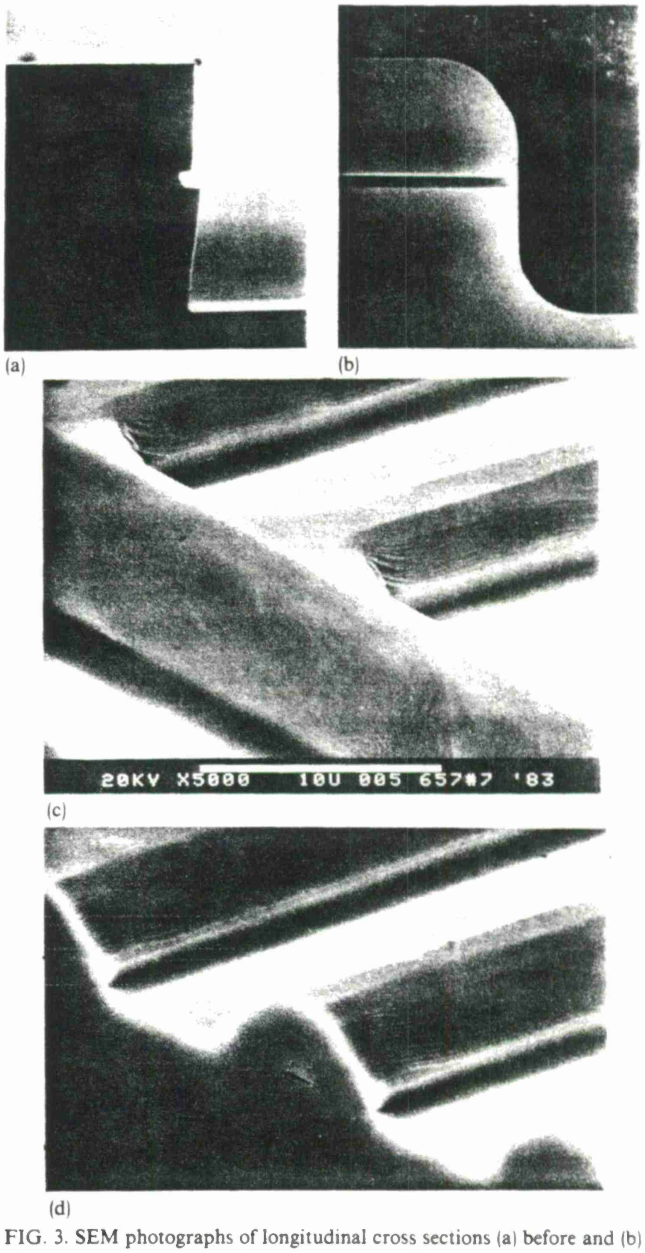


FIG. 3. SEM photographs of longitudinal cross sections (a) before and (b) after the mass transport and perspective views of (c) the transported and (d) cleaved mirrors. Except for (a), the samples have been stained in order to delineate the exposed quaternary regions, if any. Samples (a) and (b) are from wafer 644, whose active layer is 0.28 $\mu$m in thickness, and (c) and (d) are from wafer 657.

In conclusion, very low threshold current and high device yield have been obtained for GaInAsP/InP BH lasers with a chemically etched and mass-transported mirror. This result is highly encouraging and the new technique should help realize the full potential of the etched mirrors for high performance lasers and integrated optoelectronics applications.

The authors wish to thank D. E. Mull for growth and characterization of the double heterostructure wafers and for making the photolithographic masks, L. J. Missaggia for device processing and testing, W. F. McBride for device

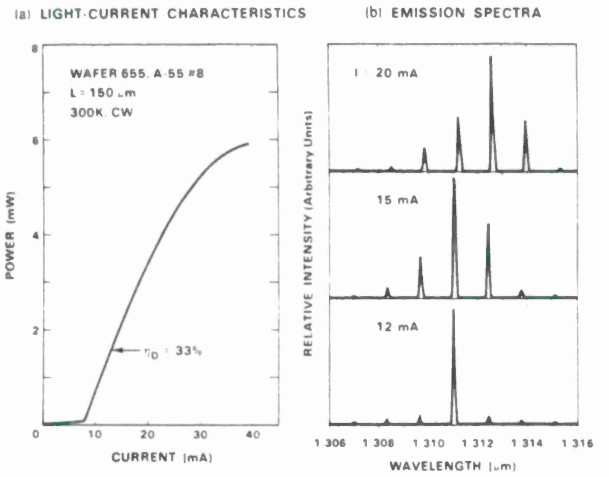


FIG. 4. Light-current characteristic and emission spectra of a GaInAsP/InP BH laser with a transported mirror.

packaging, G. W. Iseler for InP substrates, and P. M. Nitishin for part of the SEM work. At the time of this writing, it has come to the authors' attention that L. A. Coldren and coworkers have independently applied the mass-transport technique in a somewhat different manner to fabricate etched mirrors. This work was supported by the Department of the Air Force.

[1]K. Iga and B. I. Miller, IEEE J. Quantum Electron. **QE-18**, 22 (1982); and earlier works cited therein.
[2]P. D. Wright, R. J. Nelson, and R. B. Wilson, IEEE J. Quantum Electron. **QE-18**, 249 (1982); and earlier works cited therein.
[3]L. A. Coldren, K. Furuya, B. I. Miller, and J. A Rentschler, IEEE J. Quantum Electron. **QE-18**, 1679 (1982); and earlier works cited therein.
[4]S. Adachi, H. Kawaguchi, K. Takahei, and Y. Noguchi, J. Appl. Phys. **52**, 5843 (1981).
[5]O. Mikami, H. Akiya, T. Saitoh, and H. Nakagome, Electron. Lett. **19**, 213 (1983).
[6]N. Bouadma, J. Riou, and J. C. Bouley, Electron. Lett. **18**, 879 (1982).
[7]H. Blauvelt, N. Bar-Chaim, D. Fekete, S. Margalit, and A. Yariv, Appl. Phys. Lett. **40**, 289 (1982).
[8]U. Koren, Z. Rav-Noy, A. Hasson, T. R. Chen, K. L. Yu, L. C. Chiu, S. Margalit, and A. Yariv, Appl. Phys. Lett. **42**, 848 (1983).
[9]K. Furuya, L. A. Coldren,B.I. Miller, and J. A. Rentschler, Electron. Lett. **17**, 582 (1981).
[10]L. A. Coldren, K. Furuya, and B. I. Miller, J. Electrochem. Soc. **130**, 1918 (1983).
[11]S. E. H. Turley and P. D. Greene, J. Cryst. Growth **58**, 409 (1982).
[12]P. Buchmann and A. J. N. Houghton, Electron. Lett. **18**, 850 (1982).
[13]See, for example, M. Hirao, A. Doi, S. Tsuji, M. Nakamura, and K. Aiki, J. Appl. Phys. **51**, 4539 (1980).
[14]See, for example, H. Ishikawa, H. Imai, T. Tanahashi, K. Hori, and K. Takahei, IEEE J. Quantum Electron. **QE-18**, 1704 (1982).
[15]Z. L. Liau and J. N. Walpole, Appl. Phys. Lett. **40**, 568 (1982).
[16]T. R. Chen, L. C. Chiu, K. L. Yu, U. Koren, A. Hasson, S. Margalit, and A. Yariv, Appl. Phys. Lett. **41**, 1115 (1982).
[17]P. C. Chen, H. D. Law, E. A. Rezek, and J. Weller, *Technical Digest, IOOC* '83 (IECE of Japan, Tokyo, 1983) p. 190.
[18]Z. L. Liau, J. N. Walpole, and D. Z. Tsang, *Technical Digest, IOOC* '83 (IECE of Japan, Tokyo, 1983) p. 152.
[19]I. Mito, M. Kitamura, K. Kaede, Y. Odagiri, M. Seki, M. Sugimoto, and K. Kobayashi, Electron. Lett. **18**, 2 (1982).
[20]T. P. Lee, C. A. Burrus, J. A. Copeland, A. G. Dentai, and D. Marcuse, IEEE J. Quantum Electron. **QE-18**, 1101 (1982).

# REPORT DOCUMENTATION PAGE

1a. REPORT SECURITY CLASSIFICATION
Unclassified

1b. RESTRICTIVE MARKINGS

2a. SECURITY CLASSIFICATION AUTHORITY

2b. DECLASSIFICATION/DOWNGRADING SCHEDULE

3. DISTRIBUTION/AVAILABILITY OF REPORT
Approved for public release; distribution unlimited.

4. PERFORMING ORGANIZATION REPORT NUMBER(S)

5. MONITORING ORGANIZATION REPORT NUMBER(S)
ESD-TR-87-051

6a. NAME OF PERFORMING ORGANIZATION
Lincoln Laboratory, MIT

6b. OFFICE SYMBOL *(If applicable)*

7a. NAME OF MONITORING ORGANIZATION
Electronic Systems Division

6c. ADDRESS *(City, State, and Zip Code)*
P.O. Box 73
Lexington, MA 02173-0073

7b. ADDRESS *(City, State, and Zip Code)*
Hanscom AFB, MA 01731

8a. NAME OF FUNDING/SPONSORING ORGANIZATION
Rome Air Development Center

8b. OFFICE SYMBOL *(If applicable)*
RADC/ESMS

9. PROCUREMENT INSTRUMENT IDENTIFICATION NUMBER
F19628-85-C-0002

8c. ADDRESS *(City, State, and Zip Code)*
Griffiss AFB
New York, NY 13440

10. SOURCE OF FUNDING NUMBERS

| PROGRAM ELEMENT NO. | PROJECT NO. | TASK NO. | WORK UNIT ACCESSION NO. |
|---|---|---|---|
| 62702F, 61102F | 85 | | |

11. TITLE *(Include Security Classification)*
Electrooptical Devices

12. PERSONAL AUTHOR(S)
Tsang, Dean Z. and Williamson, Richard C.

| 13a. TYPE OF REPORT | 13b. TIME COVERED | 14. DATE OF REPORT *(Year, Month, Day)* | 15. PAGE COUNT |
|---|---|---|---|
| Annual Report | FROM 10/1/83 TO 9/30/84 | 1984, September, 30 | 64 |

16. SUPPLEMENTARY NOTATION
None

| 17. COSATI CODES | | |
|---|---|---|
| FIELD | GROUP | SUB-GROUP |
| | | |
| | | |

18. SUBJECT TERMS *(Continue on reverse if necessary and identify by block number)*
electrooptical devices
buried heterostructure
double-heterostructure
etched mirror laser
Q-switched diode lasers
GaInAsP/InP lasers

19. ABSTRACT *(Continue on reverse if necessary and identify by block number)*

This report covers work carried out with support of the Rome Air Development Center during the period 1 October 1983 through 30 September 1984.

GaInAsP/InP buried-heterostructure lasers formed by thermally transported InP have resulted in low threshold, high efficiency, and high device yield. Zinc diffusion has been utilized to improve the light-current linearity and reduce the threshold temperature dependence.

A technique has been developed to calculate the voltage and current distributions in the mass-transported GaInAsP/InP buried-heterostructure lasers. It is valuable for designing lasers for operation without current leakage through the InP pn homojunctions formed in the transported regions.

Mass-transported GaInAsP/InP buried-heterostructure lasers with low threshold currents and a linear light output to greater than 13 mW per facet have been obtained. This is achieved by using sufficient p-doping in the cap layer of the starting double-heterostructure wafer.

Buried-heterostructure, actively Q-switched diode lasers have been made with threshold currents as low as 14 mA. The lasers operate continously at room temperature. Full on/off modulation has been observed at measurement-limited rates of about 12.6 GHz while modulation has been seen at rates of 13.5 GHz.

The InP mass-transport technique has been used to improve chemically etched mirrors for GaInAsP/InP buried-heterostructure lasers. Devices with one such mirror and a second cleaved mirror show high device yield, threshold currents as low as 5 mA, and differential quantum efficiency as high as 33 percent.

20. DISTRIBUTION/AVAILABILITY OF ABSTRACT
☐ UNCLASSIFIED/UNLIMITED ☒ SAME AS RPT. ☐ DTIC USERS

21. ABSTRACT SECURITY CLASSIFICATION
Unclassified

22a. NAME OF RESPONSIBLE INDIVIDUAL
Lt. Col. Hugh L. Southall, USAF

22b. TELEPHONE *(Include Area Code)*
(617) 981-2330

22c. OFFICE SYMBOL
ESD/TML